# Unrest and Eruption Forecasting

9

## 9.1 Introduction

The shallow accumulation and/or transfer of magma commonly result in anomalous geodetic, geophysical or geochemical activity of the volcano, named unrest, which is detectable through a monitoring system. At closed conduit volcanoes, every eruption is preceded by unrest. However, not all unrest culminates into eruption, as unrest may also vanish back into quiescence. Therefore, deciphering the monitoring signals captured during unrest is probably the main challenge for volcanology. This in fact allows not only understanding magmatic processes, but also forecasting impending eruptions and the possible location for the opening of vents. The recent boost in the quantity and quality of monitoring data, based on key multi-parameter sets, significantly contributes to face this challenge towards enhanced understanding and more accurate and reliable eruptive forecast: the future for this exciting field looks definitely promising.

This chapter merges knowledge from all the previous chapters, highlighting the contribution of volcano-tectonics in defining unrest, its triggering mechanisms, processes and outcomes. Then it discusses how this knowledge merges into hazard assessment for risk mitigation and, in particular, in the art of forecasting eruptions, with an overview of current forecasting approaches.

The main aims of this chapter are to:

- define unrest behaviours and related processes;
- discuss the conditions triggering unrest;
- merge this knowledge into hazard assessment, also introducing key principles;
- summarize current long- and short-term forecasting approaches.

## 9.2 General Features

Volcanoes spend most of their lives in a state of **quiescence**, that can be defined as a background or baseline level characterized by a stationary state, during which measurable parameters including deformation, seismicity, or degassing activity show little or no variation. Quiescence can last for years, decades, centuries or more, depending on the type of volcano, and may be even accompanied by different manifestations in different volcanoes. For example, at a given stratovolcano with closed conduit the quiescence state is usually characterized by little or no seismicity, deformation and degassing: this may be the case of Vesuvio (Italy), from 1944 to the present. At calderas, the baseline may be defined less easily. In fact, many calderas, especially those defined as restless, do not really experience


V. Acocella, *Volcano-Tectonic Processes*, Advances in Volcanology,
https://doi.org/10.1007/978-3-030-65968-4_9

a truly quiescent state, being characterized by minor vertical deformation (often subsidence), sporadic seismicity and minor degassing activity. These features have been for example observed at Askja (Iceland) in most of the last century or at Campi Flegrei (Italy) between 1985 and 2005. These minor monitoring variations may be interpreted as the baseline for quiescence of restless calderas, provided that they are not indicative of shallow magma accumulation or transfer, or of any hydrothermal change. In fact, the fundamental point is that, regardless of the type of volcano, the baseline for quiescence should represent a state characterized by the absence of magma accumulation and/or transfer within the shallow plumbing system, as well as by the absence of important variations in any hydrothermal system.

**Unrest** is a state of the volcano, lasting from weeks to decades, characterized by an evident deviation of the monitoring parameters from the baseline (Newhall and Dzurisin 1988). This deviation may be the result of several processes, of magmatic, hydrothermal or tectonic nature, although it is most commonly related to the shallow emplacement or accumulation of magma or of magmatic and hydrothermal fluids, or to shallow magma transfer. The term "shallow" here refers to crustal depths located between the magma chamber and the surface, thus including the plumbing system in between. The shallow accumulation or transfer of magma during unrest induces stress perturbations which may promote several phenomena within the host rock. In the crustal volume surrounding the intrusion, fractures may be generated and/or reactivated, and their formation detected at the surface as swarms of volcano-tectonic earthquakes. Fracturing also changes the permeability of the host rock, affecting the shallow migration of magmatic fluids and their interaction with fluids of meteoric origin. This may induce pressure changes in any hydrothermal system, ultimately resulting in fluctuations of the composition and fluxes of the gases detected at the surface. Shallow magma and fluid emplacement or transfer also generates surface displacement. The more voluminous the intrusion, the larger the displacement, while deeper intrusions induce a weaker, albeit wider, displacement. Therefore, shallow magma accumulation or transfer can be detected at the surface through the variations in the geodetic, geophysical and geochemical monitoring signals, identifying the state of unrest (Fig. 9.1; Hill et al. 2002). These phenomena represent a simple and common, although not exclusive, sequence of magmatic and hydrothermal processes possibly occurring during unrest. In turn, unrest processes may be characterized by a wide variability of manifestations, occurring in isolated or multiple discrete events, being weaker, more intense, shorter, longer or delayed by the response of the system. Given this variability, and given the difficulty in detecting and interpreting the produced signals, the definition and duration of unrest encompass a broad spectrum of conditions which are usually defined on subjective basis. Nevertheless, efforts have been also made to codify these conditions, for communication among volcanologists as well as to authorities. A result is the definition of the Volcanic Unrest Index (VUI), whose purpose is to provide a semi-quantitative rating of unrest intensity relative to each volcano's past level of unrest and to that of analogous volcanoes (Potter et al. 2015). The VUI, calculated using a worksheet of observed phenomena, can be also determined retrospectively for historical unrest, based on qualitative information, as well as for recent episodes, based on monitoring data.

As related to shallow magma and fluid accumulation or transfer, unrest is a necessary pre-eruptive step. Indeed, any volcano usually experiences some sort of unrest before erupting, although in a few cases (especially at open conduit volcanoes, see below) this may not be easily detected. Despite the common occurrence of unrest before eruptions, unrest culminates into eruption (**eruptive unrest**) only in some cases, while in others the accumulated or transferred magma does not feed any eruption and the system returns to quiescence (**non-eruptive unrest**).

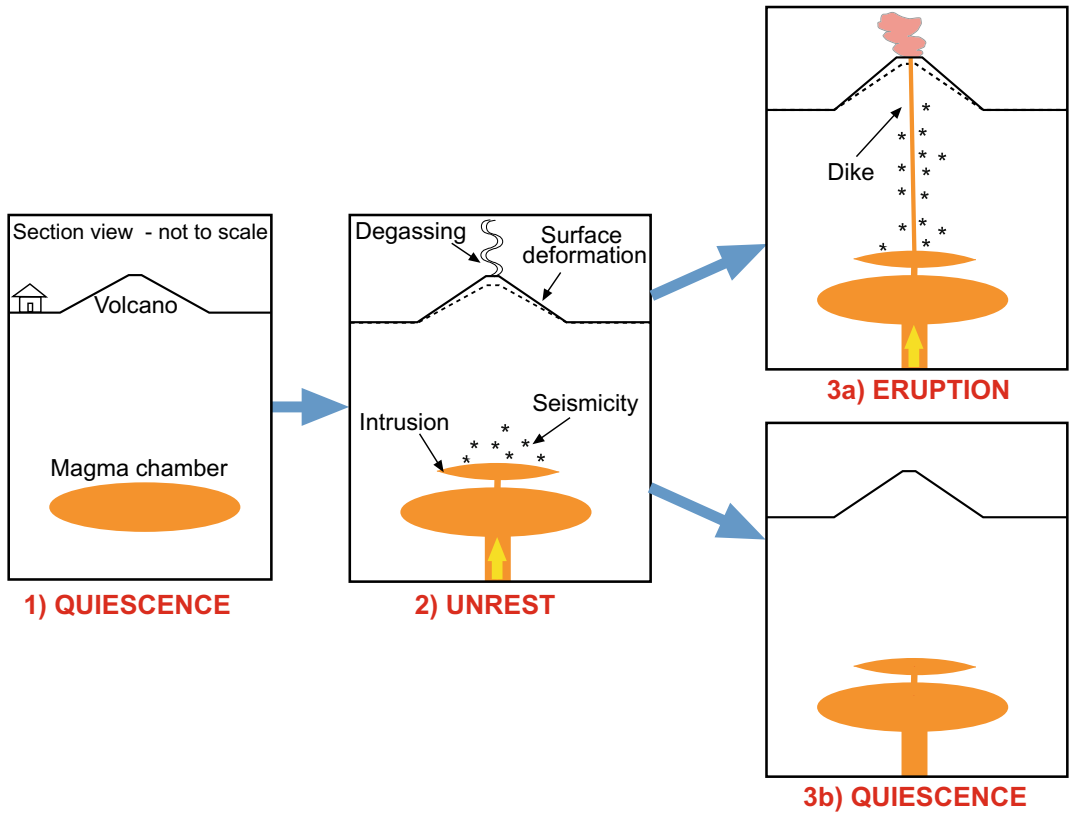


**Fig. 9.1** Unrest commonly results from shallow magma accumulation (intrusion) and is associated with surface deformation, seismicity and degassing. Unrest may culminate in eruption, if the accumulated magma reaches the surface through a dike, or turn back into quiescence, if the accumulated magma solidifies

For example, the island of El Hierro (Canary Islands) experienced more than 3 months of eruptive unrest in 2011 (Fig. 9.2; Lopez et al. 2012). In mid-July, tens of seismic events per day were detected. These then increased to hundreds of seismic events per day (maximum magnitude was 2.7) below the northern part of the island, at 10–15 km of depth. Anomalous $CO_2$ degassing and slight inflation were detected at the surface. Throughout September seismicity increased considerably (maximum magnitude $M$ was 3.3) and migrated southward, accompanied by increased inflation rate and $^{222}Rn$ emission. In late September-early October seismicity accelerated in frequency and magnitude (maximum magnitude was 3.7), focusing at 12–14 km of depth. Deformation also accelerated, with sudden inflation, deflation and re-inflation, accompanied by an increase in the $^{222}Rn$ emission. In the two days before the eruption deformation and seismicity continued to increase. The maximum magnitude reached 4.7 at 12 km depth, shallowing, a few hours later, between 6 and 1 km to the south of the island, suggesting dike ascent. Seismicity then turned into tremor, suggesting the onset of a submarine eruption a few kilometres off the south coast, along the feeding system of the southern ridge of the island. The submarine eruption lasted for 5 months and was then followed, for nearly 2 years after the eruption, by several sill-like intrusions, each emplaced at 13–16 km of depth between 3 and 20 days (Benito-Saz et al. 2019).

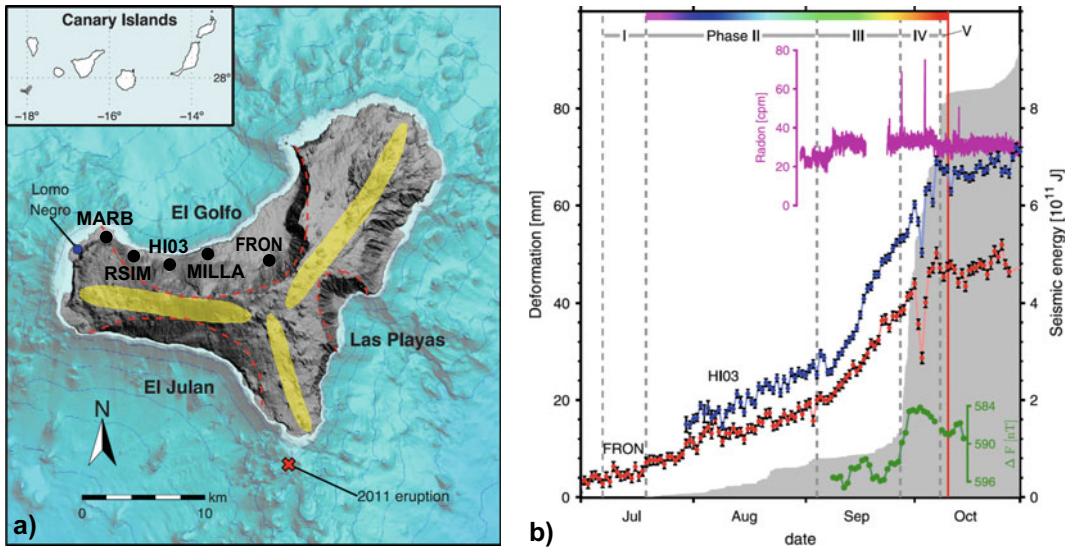


**Fig. 9.2** The 2011 El Hierro (Canary Islands) unrest. a) DEM of El Hierro and its surrounding bathymetry. The three main rift zones (yellow) and collapse scarps (red lines), and the location of the last inland eruption (blue dot) and the 2011 eruption (red cross) are shown. b) Evolution of monitored parameters from July to October 2011. Grey shading shows accumulated seismic energy. Red and blue points show he northing displacement of GPS stations with error bars (1σ). The difference between MLLA and MARB magnetic stations is plotted as green dots. The $^{222}$Rn temporal variation in RSIM is shown in magenta. Red vertical line marks eruption onset (modified after Lopez et al., 2012)

Conversely, Alcedo caldera (Galapagos) experienced non-eruptive unrest between 2007 and 2011 (Fig. 9.3; Galetto et al. 2019). An initial asymmetric uplift of ∼30 cm of the southern caldera floor from 2007 to 2009 was due to the inflation of a sill and the activation of an inner ring fault. This was followed by subsidence and contemporary uplift of the northwestern caldera rim in early 2010, compatible with the withdrawal of magma from the previously inflated sill through its lateral migration to the northwest. Then, from June 2010 through March 2011, caldera uplift resumed, consistent with the repressurization of the previously inflated sill, although without promoting further shallow magma transfer. This evolution suggests episodic magma accumulation in a shallow reservoir beneath the caldera, with aborted lateral magma migration due to discontinuous or weak magma supply.

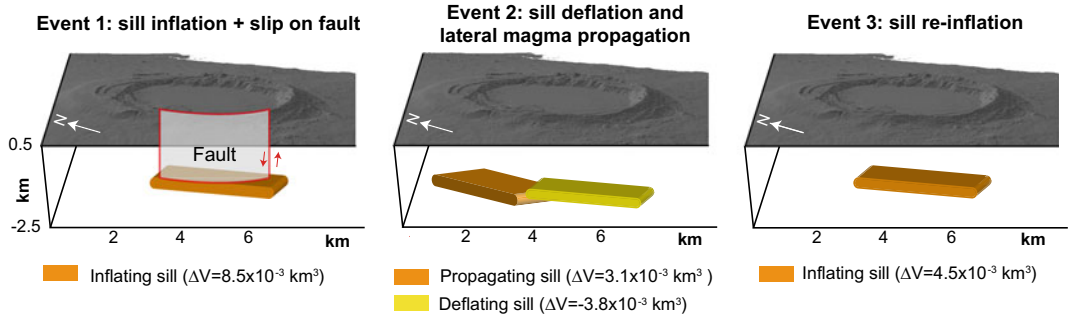


**Fig. 9.3** The three deformation events due to magma emplacement and transfer, with the related volume variations $\Delta V$, during the 2007–2011 non-eruptive unrest at Alcedo caldera (Galapagos; modified after Galetto et al. 2019)

More in general, on average 36% of unrest episodes at 228 volcanoes between 2000 and 2011 have not culminated into eruptions, a percentage lowering to 14% for shield volcanoes and rising to 48% for calderas (Phillipson et al. 2013). Therefore, as eruptions are usually preceded by unrest, but unrest does not necessary culminate into eruption, unrest represents a necessary but not sufficient condition for eruption. In fact, to erupt, the magma responsible for unrest must be able to reach the surface, a condition difficult to define a priori, causing significant uncertainty in forecasting any impending eruption. For a first-order understanding and also forecast, a fundamental distinction is to try to define whether unrest mainly results from (a) shallow storage (emplacement or accumulation) of magma or, conversely, also from (b) shallow transfer (including the rise) of magma towards the surface, typically through a dike. Based on the identification of the dominant process, it may be in principle possible to forecast an impending eruption. Diagnostic criteria to determine whether magma is accumulating or transferring during unrest may be given by the monitoring data. As anticipated in Sect. 8.3.2, the surface deformation pattern resulting from shallow magma accumulation (induced by spherical or elliptical reservoirs and sills) shows radial symmetry, where the similar vertical or horizontal component of the radial displacements at the surface identifies an axisymmetric pattern. Conversely, the surface deformation pattern induced by shallow magma transfer (i.e., a propagating dike) shows non-radial symmetry (non-axisymmetric displacement), being the vertical and horizontal displacements directional. Seismicity may also provide important clues, in terms of spatial patterns and seismic signals. The seismicity due to the shallow rise of magma may be highlighted by an upward migrating pattern of volcano-tectonic earthquakes becoming progressively dominated by long-period and very long-period earthquakes, and tremor.

Therefore, it is possible to distinguish a quiescent volcano from a volcano experiencing unrest, and within unrest, it may be possible to distinguish shallow magma accumulation from shallow magma transfer, the latter heralding an impending eruption. The conditions related to **magma accumulation** may show larger variability in intensity than those related to shallow magma transfer (Fig. 9.4). For example, unrest may be characterized by small amplitude and low rate deformation, with overall radial symmetry, low-level seismicity, and degassing anomalies related, in composition and rate, to the less soluble fluids (as $CO_2$). This condition has been occurring in many, probably most, unrest episodes, especially at felsic calderas, as for example at Santorini (Greece) in 2011 or Campi Flegrei between 2012 and 2013 (Parks et al. 2012; D'Auria et al. 2015; Chiodini et al. 2015). In other cases, unrest may be characterized by a larger deformation (in terms of both amplitude and rate) with radial symmetry at the surface, more intense seismicity (both in number and magnitude of earthquakes) and an increase in the degassed fluxes, possibly also characterized by more soluble species (as $SO_2$). These more intense conditions may be recognized a few weeks before an eruption, when a significant amount of magma accumulates at shallow levels fracturing the host rock, inducing seismicity and gas release, as for example observed at Mount St. Helens (Washington, USA) in 1980 or at Pinatubo (Philippines) in 1991 (Lipman and Mullineaux 1981; Newhall and Punongbayan 1996). Nevertheless, in some cases these intense conditions may even last for a few years without necessarily culminating into eruption, as for example observed between 1982 and 1984 at Campi Flegrei and 1983 and 1985 at Rabaul (Papua New Guinea; Acocella et al. 2015, and references therein). Despite the variability in the intensity of the monitoring parameters, or in their accelerating or decelerating trends, the radial symmetry of the deformation and the persistence of the seismicity in a specific crustal volume remain the features which may allow interpreting unrest as resulting from shallow magma accumulation. Available data suggest that such a magma accumulation commonly occurs in sill-like bodies at the top of the magma chamber.

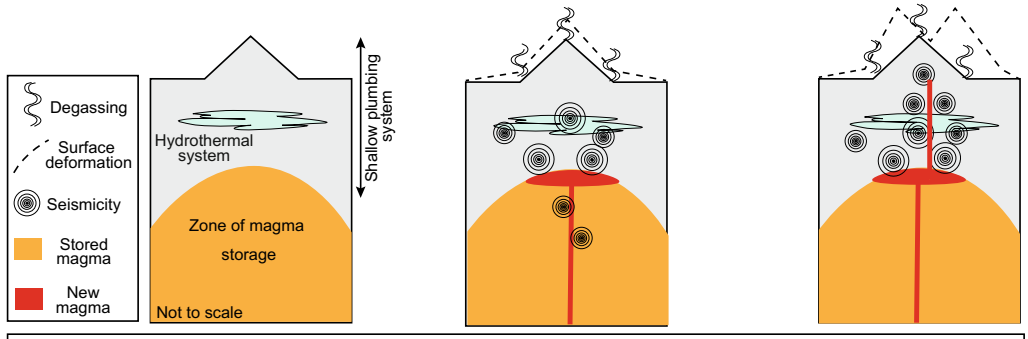


| | | | |
|---|---|---|---|
| **DEFORMATION** | None, or subsidence | Radial symmetry<br>Uplift mm/yr ↔ Uplift m/yr | Non-radial symmetry<br>Uplift ≥ m/yr |
| **SEISMICITY** | None | Above intrusion, stationary<br>Few events/month ↔ $10^3$ events/month<br>VT, deep LP ↔ VT, deep LP, shallow LP? VLP? ULP? Tremor? | Above intrusion, widening / migrating<br>VT, shallow LP, VLP, ULP, tremor |
| **DEGASSING** | $CO_2$ | $CO_2$ (magmatic component), $SO_2$? | $CO_2$, $SO_2$, HCL, HF |
| **DURATION** | Years to thousand years | Months to years | Days |
| **PROCESS** | No shallow magma accumulation nor transfer | Shallow magma accumulation | Shallow magma transfer |
| **STATE** | **Quiescence** | **Unrest: magma accumulation** | **Unrest: impending eruption** |

Facts / Interpretation

**Fig. 9.4** The states of a volcano while not erupting: quiescence, magma accumulation and magma transfer. Indicative monitoring parameters to define these states are usually expressed as orders of magnitude. Seismicity: VT (volcano-tectonic), LP (long-period), VLP (very long-period), ULP (ultra long-period); the orange area in the diagrams indicates a magma reservoir with mush and melt zones. See text for details

Conversely, the appearance of deformation with non-radial symmetry and any variation in the distribution of seismicity, possibly evolving in a migrating pattern, are indicative of a shallow **magma transfer** during unrest. As this state likely anticipates eruption, it may be defined of impending eruption (Fig. 9.4). This is commonly characterized by dike propagation: dikes may propagate vertically, feeding eruptions within a volcanic edifice, or horizontally, erupting at a distal location, as observed on the slopes of (mainly mafic) volcanoes or along rift zones. Dikes usually nucleate from magma chambers, or other zones of shallow accumulation, and reach the surface within a few days. However, their nucleation and propagation do not necessarily guarantee that magma will reach the surface and erupt, as dikes may stall at depth. Therefore, the state of impending eruption represents more precisely a state of probable eruption. As it is difficult to determine if a nucleated dike will reach the surface and feed an eruption, the fundamental point here is that dike propagation marks a change in the state of a volcano, which passes from shallow magma accumulation to magma transfer towards the surface. From the risk mitigation perspective, these two states significantly differ, as magma transfer should require the activation of all the operational procedures needed to mitigate risk, including evacuation.

The transitions between these quiescence, accumulation and transfer states, though grounded on variations of observables and/or monitoring parameters, cannot be simply defined detecting pre-defined values or thresholds. In fact, there is usually no default and unique value which defines a priori a specific state of a

volcano, and even less for groups of volcanoes. Rather, a range of monitoring values, also varying over an order of magnitude, may better characterize the transitions between the volcano states (Fig. 9.4).

As anticipated, in some cases it is difficult to detect unrest. While unrest is more intense and evident at monitored volcanoes with closed conduit, at some closed conduit volcanoes unrest may consist of extremely short (hours or days) and subtle variations. This condition is sometimes explained by retrograde or **second boiling** of the previously accumulated magma, which cools and crystallizes, enriching the residual liquid in gas and promoting gas exsolution. The result may be a sudden explosive eruption, as proposed for Kalud (Indonesia) in 2014 and Calbuco (Chile) in 2015, both explained by an internal trigger, suggesting that closed-conduit systems can evolve into an explosive eruption with very little precursory warning (i.e., unrest; Arzilli et al. 2019; Cassidy et al. 2019). Conversely, at open conduit volcanoes, the magma usually emplaces and rises to the surface without significant pressure build up and thus with limited deformation of the host rock. Therefore, here both the surface deformation and seismicity may be limited or absent, providing subtle information to detect any unrest and even impending eruption. In case the vertical open conduit resembles a pipe and becomes pressurized, any deformation may also have radial symmetry, similar to that of accumulating sources and thus potentially masking the rise of magma. However, as open conduit volcanoes degas significantly, the composition and flux of the degassed species may be indicative of the depth of the magma, as gas solubility within magma mainly depends on pressure: therefore, degassing variations may reveal the rise of magma at open conduit volcanoes (see Sect. 8.5).

## 9.3 Unrest Triggers

Unrest may result from magmatic, hydrothermal and tectonic processes (e.g., Newhall and Dzurisin 1988). Magmatic processes are those involving magma emplacement or transfer and in which magma, thermal energy and magmatic volatiles enter the shallow plumbing system (see Sect. 9.3.1). Hydrothermal processes are those involving the dynamics of the hydrothermal system and subsurface aquifers, in which the physical or chemical state of fluids is changed by interaction with magmatic fluids or through heating driven by magma-related thermal anomalies (see Sect. 9.3.2). In principle, variations in the microgravity field during unrest may allow discriminating the density of the responsible source, and thus its magmatic or hydrothermal nature (see Sect. 8.4.2; Battaglia et al. 1999; Tizzani et al. 2009). Tectonic processes occur in country rocks and dominantly involve changes in mechanical energy, with little or no movement of mass into or out of the subvolcano environment: these commonly derive from external forcing. A tectonically-driven unrest typically results from the shorter-term (transient passage of seismic waves) and/or longer-term (stress accumulation) variations associated with nearby regional tectonic earthquakes. These variations may affect the hydrothermal and/or the magmatic system of the volcano, eventually leading to unrest and eruption (see Sect. 9.3.3; Hill et al. 2002; Manga and Brodsky 2006).

Probably, the anomalies signalling unrest are never purely magmatic, purely hydrothermal or purely tectonic, as for example a magmatic unrest may affect also the hydrothermal system, whereas a tectonically-driven unrest may affect both the magmatic and hydrothermal systems. However, when clearly established, the cause of unrest usually involves the accumulation and/or transfer of magma (or magmatic fluids) within the shallow plumbing system of the volcano (Newhall and Dzurisin 1988; Phillipson et al. 2013; Acocella et al. 2015). The possible triggering factors of unrest, as well as the related processes, are described separately below.

### 9.3.1 Magmatic Trigger

Shallow magma accumulation is probably the most common cause of unrest. In fact, available

evidence suggests that the direct rise of magma via dikes from deeper reservoirs without any shallow storage is not frequent, and usually the deep magma stops ascending and emplaces at shallow levels. In particular, following vertical transfer from the deeper plumbing system, magma often accumulates at a few kilometres of depth, often at the top of a magma chamber. The deeper transfer may pass unnoticed, because occurring at greater depth (limiting surface deformation and degassing), at higher temperature (limiting seismicity) and masked by shallower magma emplacement (limiting again surface deformation). Magma commonly emplaces through sills and eventually accumulates developing laccoliths. These intrusion shapes are justified by available field evidence of shallow plumbing systems and eroded magma chambers, as well as deformation and geophysical data (see Chap. 4). Sill emplacement is commonly accompanied by fracturing of the nearby host rock, focused above the sill and around its lateral terminations, detected as a swarm of VT earthquakes (Fig. 9.5). As fracturing increases the permeability of the host rock to magmatic fluids, it may also increase the degassed fluxes at the surface. In addition to seismicity and degassing, magma accumulation usually induces surface deformation with radial symmetry and microgravity changes suggesting magma addition. A hydrothermal system may amplify or buffer these monitoring signals. In principle, as previously anticipated, it is expected that the increased permeability following the fracturing generated by the accumulation of magma releases magmatic gases. These gases may reach and pressurize the hydrothermal system, in turn triggering shallower seismicity, increased degassing (where the magmatic component becomes diluted) and surface deformation, amplifying the effects due to magma accumulation alone. However, a hydrothermal system may also buffer the signals deriving from magma accumulation, for example, acting as a high permeability medium, releasing the fluids and relaxing the surface deformation. Also, some magmatic gases indicating the rise of magma, as $SO_2$, may be scrubbed by hydrothermal systems and be undetected at the surface. These mixed possibilities warn against assuming an a priori expected role of the hydrothermal system during shallow magma accumulation.

A crucial feature controlling the fate of a magmatically-triggered unrest is the eruptibility of the accumulated magma. Under which

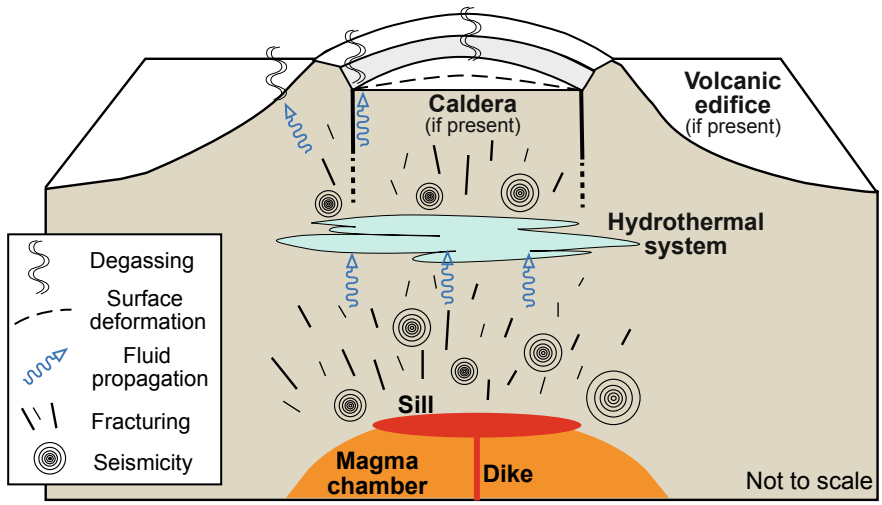


**Fig. 9.5** Possible processes involved in unrest triggered by magma accumulation through an inflated sill. Magma accumulation may induce fracturing and thus variations in the permeability of the host rock, also resulting in fluid migration and, in turn, pressure variations within a hydrothermal system. At the surface, these processes manifest through seismicity, deformation, and degassing (modified after Acocella et al. 2015)

conditions does the magma rising from depth arrest, emplace, accumulate, and then eventually rise again towards the surface? This behaviour, which ultimately distinguishes eruptive from non-eruptive unrest, may depend upon several conditions, which can be largely reconciled with those promoting dike propagation, sill formation and dike nucleation (see Sects. 3.4, 3.5, 4.3 and 4.6.3). As explained in the previous chapters, unless a dike propagating from depth has significant overpressure, it will likely stall at some shallow crustal level and there possibly emplace feeding a sill, promoting unrest. Magma emplacement may preferably occur in correspondence of mechanical and thermal barriers, as for example along the major rigidity and viscosity contrasts at the top of magma chambers. The stronger the barrier with regard to the magma overpressure, the longer the magma accumulates. However, if magma supply is low or discontinuous, magma accumulation may cease, with the volcano returning to quiescence. Conversely, the stronger the magma overpressure with regard to a barrier, the easier is for the emplaced magma to propagate towards the surface, feeding an eruption. These balances should be also considered through time, with evidence suggesting that magma eruptibility decreases with the duration of unrest (see Sect. 9.4). Determining and quantifying the conditions controlling magma eruptibility and establishing their relative importance in general and specific situations should be a major topic for future research.

### 9.3.2 Hydrothermal Trigger

In some instances, magma does not appear directly involved as a cause of unrest, either because it does not directly participate in the process or because it is not possible to prove its involvement. In this case, in absence of remote tectonic triggers, a leading role of the hydrothermal component in unrest may be postulated. Hydrothermally-triggered unrest does not necessarily require external input of fluids and heat, as even an internal decrease in the permeability may perturb the system. The decrease in permeability may result from the precipitation of hydrothermal minerals within the fracture network, which becomes partly obstructed (**self-sealing**), determining a transient build up in the fluids pressure. Self-sealing of hydrothermal systems may thus generate seismicity, surface deformation, degassing and, in extreme cases, also phreatic eruptions. However, as hydrothermal systems in volcanoes derive most of their energy from the underlying magma, the involvement of the hydrothermal system alone in unrest is not common. More often, a supply of heat from depth, probably related to some magmatic input or possibly only related to increased deeper crustal permeability, may pressurize the hydrothermal system, determining unrest. These conditions may for example explain the phreatic eruption occurred without evident warning at Ontake (Japan) in 2014, causing 67 victims (Fig. 9.6; Kato et al. 2015; Oikawa et al. 2016). Retrospective re-examination of the minor seismicity before the phreatic eruption allowed detecting volcano-tectonic and long-period earthquakes for at least one month before the event. This seismicity aligned along a subvertical path beneath the craters, suggesting the rise of fluids along the summit conduit. A few minutes before the phreatic eruption the seismicity migrated upward and laterally, accompanied by an accelerated increase of tremor amplitude and anomalous tiltmeter signals indicating summit upheaval. This behaviour is explained through the filling of the conduit with pressurized fluids, which propagated to the surface immediately before the eruption. While it may be argued that the unrest signals have been so subtle to be detected only retrospectively, and that the fluids derived at least in part from the magma reservoir (Miyagi et al. 2020), the Ontake event still marks a dramatic episode of rapid unrest with major involvement of the hydrothermal system. In a similar fashion, the 2004–2006 unrest at Mt. Spurr (Alaska, USA) and the 2016 unrest at Tenerife (Canary Islands) have been characterized by the rise of magmatic fluids into the hydrothermal system (Koulakov et al. 2018; D'Auria et al. 2019).

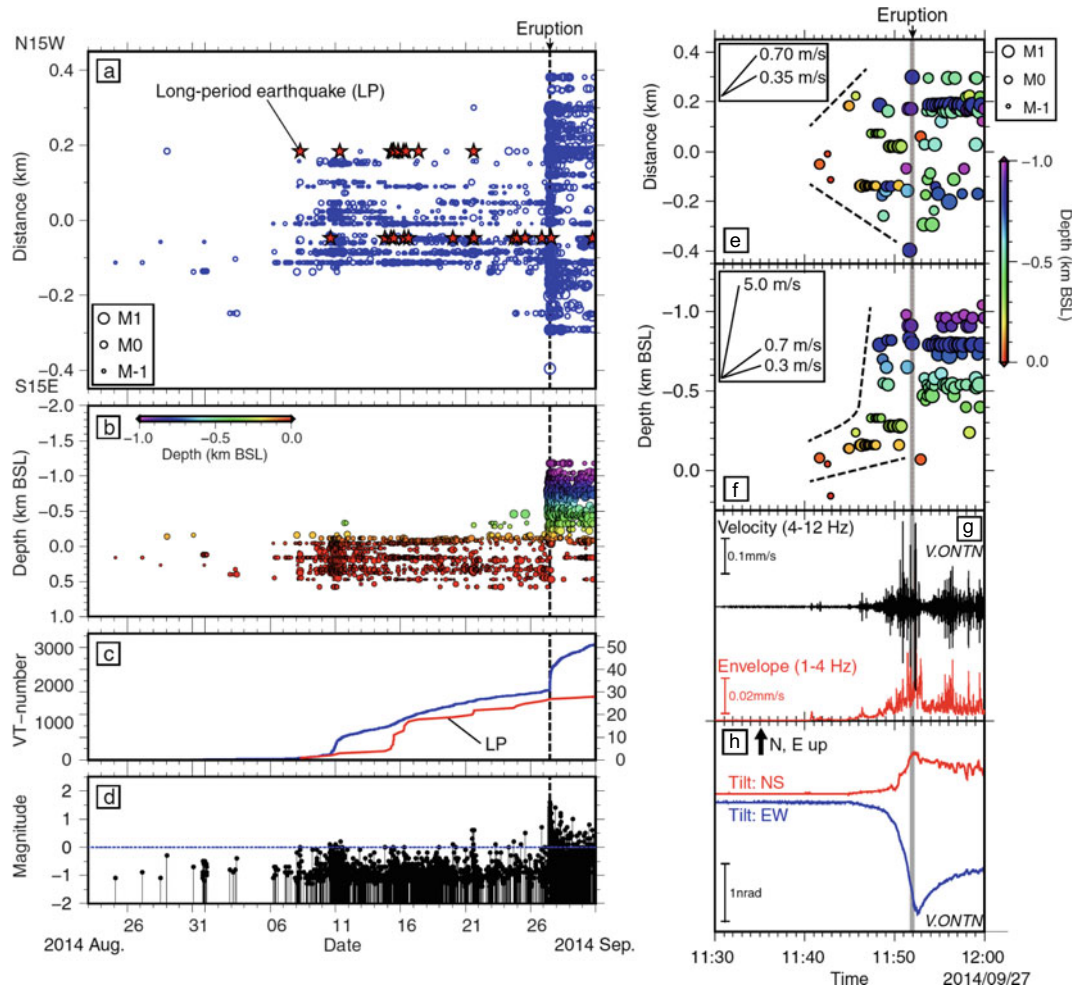


**Fig. 9.6** The 2014 Ontake (Japan) phreatic eruption. **a** to **d** Longer-term seismicity. **a** Space–time diagram of seismic events before and after the eruption (23 August-30 September), with earthquake times and locations projected onto the strike of the hypocentre alignments; blue circles = VT earthquakes; red stars = LP events. **b** Depth variations in VT earthquakes over time. Circles are scaled to magnitude and color-coded to depth, with positive values below sea level (BSL). **c** Cumulative number of VT earthquakes (blue curve) and LP events (red curve) over time. **d** Magnitude versus time. **e**–**h** Shorter-term (minutes) precursors. **e** Horizontal distance of VT earthquakes from 11:30 to 12:00 JST on 27 September, projected onto the strike of the hypocentre alignments (N15°W-S15°E). Circles are scaled to magnitude and color-coded to depth. Black dashed lines approximate the locations of the fronts of earthquake migrations. **f** Depth variations in VT earthquakes, coloured to depth. **g** Band-pass filtered waveform between 4 and 12 Hz (black curve) and envelope between 1 and 4 Hz (red curve) recorded at V.ONTN station. **h** Time series of tiltmeter records observed at V.ONTN station. NS and EW components denote the northward and eastward ground-up components, respectively (Kato et al. 2015)

### 9.3.3 Seismic Trigger

Hydrologic responses to earthquakes, including liquefaction, changes in stream and spring discharge, in the properties of groundwater, in the water level in wells, and the eruption of mud volcanoes have been all documented for thousands of years. This response has been observed also at volcanoes, where the above-mentioned processes have been commonly associated with unrest affecting the hydrothermal system and even the magma chamber, suggesting that

earthquakes influence the state of volcanoes (Wang and Manga 2010, and references therein). Indeed, studies in the last two decades have shown that far-field (i.e., regional) seismicity may trigger unrest and magmatic eruptions at nearby volcanoes. For example, a perturbation in the deformation field and increase in seismicity were detected at Long Valley caldera (California, USA) during and after the 1992 Landers earthquake, which occurred ~420 km away. This variation has been interpreted as resulting from pressure increase owing to gas bubbles, which may have been shaken loose during the passage of the seismic waves (Fig. 9.7; Linde et al. 1994).

Similarly, in September 2002 an earthquake occurring along a fault of the unstable flank of Mount Etna (Italy) was followed, one month later, by the eruption along the nearby Northeast Rift, which had been inactive for more than 50 years. The eruption in turn seismically reactivated the same fault initially responsible for the earthquake, in a context of kinematic coupling between seismicity and magmatic activity (Acocella et al. 2003). Evidence for regional earthquakes promoting volcanic or hydrothermal activity has been provided in several other cases, including the eruptions of Vesuvio in the last ~1000 years (Nostro et al. 1998), the largest historical 1707 eruption at Mount Fuji (Japan; Chesley et al. 2012) and the 2015 unrest at Deception Island (Antarctica; Almendros et al. 2018). Evidence has been also collected for a single earthquake triggering eruptions at different volcanoes, as immediately after mega-earthquakes (which are characterized by

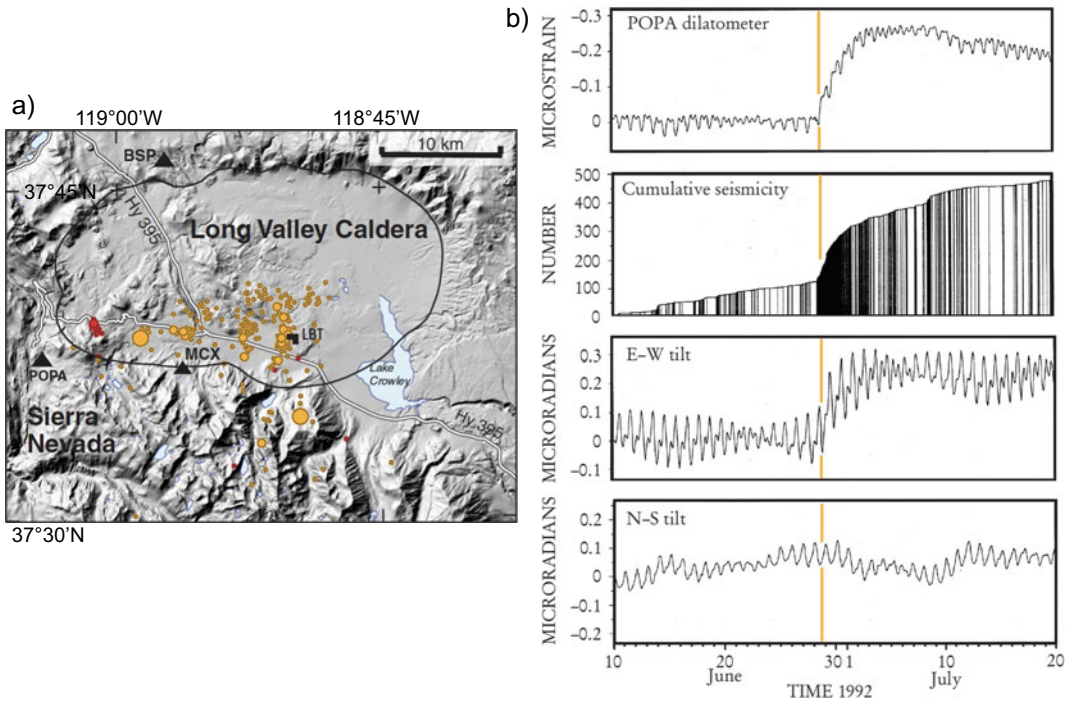


**Fig. 9.7** **a** Seismicity induced at Long Valley caldera (California, USA) by the *M7.3* Landers earthquake (28 June 1992; orange circles) and the *M7.1* Hector Mine earthquake (16 October 1999; red circles); borehole dilatometers = solid triangles; long-base tiltmeter (LBT) = inverted L. **b** Volumetric strain recorded by POPA dilatometer, cumulative number of earthquakes, and E-W and N-S components of LBT from 10 June to 20 July 1992. Negative strain is compressional; positive tilt is down to the east and north; high-frequency wiggles on the dilatometer and tiltmeter records are solid-earth tides. Orange line marks the Landers earthquake (modified after Hill et al. 2002; Linde et al. 1994)

magnitude $M > 8.5$) in Kamchatka (Russia) in 1952, in Chile in 1960, in Alaska (USA) in 1964 and in Sumatra (Indonesia) in 2004. In all these cases, the post-seismic eruptive frequency along the portion of volcanic arc closer to the hypocentre increased sensitively with regard to the pre-seismic frequency (Walter and Amelung 2007). However, not all mega-earthquakes trigger eruptions, as observed after the 2010 Maule (Chile; *M8.8*) and 2011 Tohoku (Japan; *M9.0*) earthquakes, where only minor seismicity and deflation were observed at nearby volcanoes in the months following the earthquakes. The deflation may be related to the enhanced degassing from the hydrothermal systems after the co-seismic increase in crustal permeability and/or to crustal stretching (Pritchard et al. 2013; Takada and Fukushima 2013). Recent experiments suggest that the possibility to have post-seismic eruption or instead deflation results from the different patterns (upward or downward-lateral, respectively) of the migrating fluids during an earthquake, as constrained by the oscillation frequency of the volcanic edifice with regard to its resonance frequency (Namiki et al. 2019).

In general, it has been estimated that ~0.4% of explosive volcanic eruptions occur within a few days of large, distant earthquakes. This many "triggered" eruptions is much greater than expected by chance. This behaviour is not restricted to magma, as a widespread hydrologic response to seismicity is also observed (Fig. 9.8; Linde and Sacks 1998; Montgomery and Manga 2003; Manga and Brodsky 2006; Wang and Manga 2010). In particular, the stronger the earthquake, the farther a certain magmatic or hydrologic effect can manifest, with the largest magnitude earthquakes potentially affecting magmatic activity at volcanoes nearly 1000 km distant. The highest correlation coefficients between earthquakes and eruptions are found for regions along the Pacific subduction zones, where the largest earthquakes occur (Eggert and Walter 2009). The state of the affected magma may provide another important influencing factor. Evidence from the 2015 Ambrym

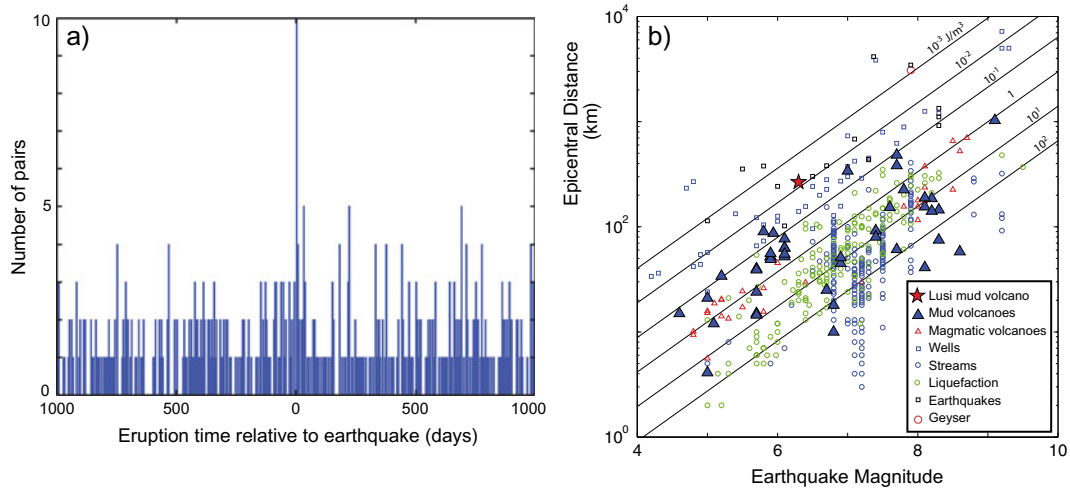


**Fig. 9.8** Time and space relationships between earthquakes and eruptions. **a** Histogram showing the number of eruptions as a function of time relative to $M > 8$ earthquakes. Negative times correspond to eruption prior to the earthquake. Only eruptions located within 800 km of the earthquake epicentre are included; bins are 5 days wide (modified after Manga and Brodsky 2006). **b** Distribution of earthquake-triggered hydrologic changes and earthquake-induced magmatic volcanic eruptions as a function of earthquake magnitude and distance. Also plotted are the log distance versus magnitude contours of constant seismic energy density, which is the seismic energy in a unit volume in the seismic wave train: this represents the maximum seismic energy available to do work at a given location during the earthquake (modified after Wang and Manga 2010; image courtesy Michael Manga)

(Vanuatu) eruption, triggered by a *M6.4* earthquake which occurred 30 h earlier, suggests that partially cooled and crystallized (i.e., $H_2O$-saturated) basaltic magmas are more susceptible to triggering from earthquakes. In fact, if the magma is too hot the stress drop required to grow the bubbles is too large, whereas if it is too cold the magma can no longer flow (Hamling and Kilgour 2020).

Several mechanisms may explain the remote triggering of unrest and volcanic eruptions, as the failure of rocks surrounding stored magma, a decrease in the deviatoric stress promoting dike propagation, changes in magma overpressure, including volatile exsolution, the growth of bubbles, the advection of large pressures by rising bubbles and overturn of magma chambers. In the case of mud volcanoes and geysers, liquefaction caused by shaking and changes in permeability by opening or creating new fractures may explain the observed hydrologic changes. All these mechanisms require a process that enhances small static stress changes caused by earthquakes or that can convert (the larger) transient, dynamic strains into permanent changes in pressure (Belardinelli et al. 2003; Manga and Brodsky 2006; Walter and Amelung 2007).

**Static stress** changes develop as a consequence of the slip of a fault during an earthquake and result in permanent perturbation of the nearby stress field. As the two sides of the fault move in opposite directions, stress is exerted parallel and perpendicular to the fault plane. When the shear stress exceeds the frictional resistance on the fault, or when the perpendicular stress is eased, the rocks on either side slip past each other suddenly, generating an earthquake. Both components of stress, which when added together are called **Coulomb stress**, diminish along the segment of the fault that slips and become redistributed to inactive zones along the same fault or to nearby faults (Fig. 9.9; Stein 2003). The local increase in Coulomb stress at these inactive zones could be sufficient to trigger successive earthquakes. To estimate if slip on a new fault is encouraged or discouraged after an earthquake, the change in Coulomb failure stress $\Delta C_{FS}$ is calculated as:

$$\Delta C_{FS} = \Delta\sigma_S + \mu(\Delta\sigma_N + \Delta P) \qquad (9.1)$$

where $\Delta\sigma_S$ is the shear stress change on a fault, $\Delta\sigma_N$ the normal stress change, $\Delta P$ the pore pressure change in the fault zone, and $\mu$ the coefficient of friction; in this approach a constant friction model is assumed (e.g. King et al. 1994; Harris 1998; Walter et al. 2005). Fault slip is encouraged if the change in Coulomb failure

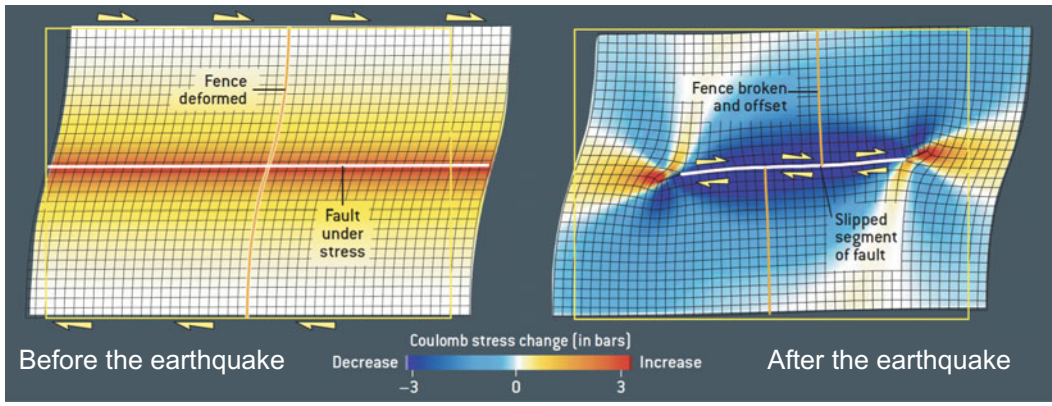


**Fig. 9.9** Conceptual model of variation of the stress accumulated along a dextral fault before and after an earthquake occurring in the central part of the fault (map view). Before the earthquake (left) the long-term accumulated stress focuses along the entire fault length. After the earthquake (right) the portion of fault that has slipped has released the stress (in blue), whereas at its lateral terminations the stresses have increased (in red) because of stress transfer (Stein 2003)

stress induced by the earthquake is positive, and discouraged if the change is negative. A change of the Coulomb failure stress by 0.1 MPa is considered significant, although stress triggering may occur even below 0.01 MPa (Stein 2004). Therefore, one can estimate if the stress perturbations induced by an earthquake may trigger slip (and thus further seismicity) on nearby faults. Indeed, the same process may also affect magmatic activity. In fact, Coulomb stresses may likewise induce pressure changes in a magma body below a volcano. Increased compressional stress in the crust surrounding a magma chamber that is close to its critical state may squeeze magma upward, whereas a decrease in compressional stress can promote magma depressurization, additional melting, the formation of bubbles as volatiles exsolve, the "unclamping" of conduits above the magma chamber, dike nucleation and propagation (Hill et al. 2002; Walter and Amelung 2007). Static stresses are, by definition, time independent and their effects may manifest immediately after the stress perturbation or even after years. The observed delays of months to years between the earthquake and the eruption are poorly understood, although diffusion of interstitial crustal fluid, mostly water, in response to static stress changes may be important.

**Dynamic stress** changes develop only during the passage of seismic waves induced by an earthquake and are thus transient, lasting from seconds to minutes. Dynamic stresses propagating through seismic waves from large earthquakes are capable of triggering other earthquakes or, in the case of volcanoes, unrest and eruption (Linde et al. 1994; Hill and Prejan 2007). Models for dynamic triggering fall under two broad groups, one appealing to Coulomb failure with various friction laws and the other appealing to the activation of hydrous or magmatic fluids. For dynamic triggering under the frictional models, the stress state in the crust must differ from the Coulomb failure stress by less than the peak amplitudes of the dynamic stresses (typically <0.1 MPa for remote triggering). These models are generally consistent with the onset of triggered seismicity during the dynamic stresses, followed by decay. Fluid excitation models involve fluid transport or a phase change. These fluid-based models, whether hydrous or magmatic, involve some crustal deformation through intrusion, pressure changes (in the case of bubble excitation), convection (in a magma body) or poroelasticity (in the case of fluid diffusion). These models admit the possibility of delayed onsets of triggered seismicity and increasing or sustained activity rates for extended periods following passage of the dynamic stresses. Extensional stress regimes hosting geothermal and volcanic activity seem more susceptible to remote dynamic triggering than compressional stress regimes, although remote triggering is not limited to extension (Hill and Prejan 2006). Dynamic models also explain most of the observed hydrologic responses, both within and beyond the near-field (Wang and Manga 2010).

Despite the common triggering capacity, static and dynamic stress changes may induce quite different effects. While a static stress change is able to advance or delay an instability depending on its sign, a dynamic stress pulse promotes nearly instantaneous failure, in case its amplitude is positive and large enough (Belardinelli et al. 2003). Also, static and dynamic stresses have different value and decay with distance. For a same earthquake, static stress changes are one order of magnitude smaller than dynamic stresses within $10^2$ km from the hypocentre (Table 9.1; Manga and Brodsky 2006). This difference increases with distance $s$, so that static stress changes become four orders of magnitude smaller than dynamic stresses at $10^4$ km from the hypocentre. This follows from the fact that while static stresses fall off as $1/s^3$, dynamic stresses fall off as $1/s^{1.66}$. Therefore, dynamic stresses may propagate to longer distances and may be still important where static stress become negligible. For example, the simultaneous occurrence of two eruptions (Stromboli and Etna) and one unrest (Panarea Island) in late 2002 in the

**Table 9.1** Static and dynamic stress changes induced by a *M8* earthquake as a function of the distance from the hypocentre (modified after Manga and Brodsky 2006)

| Forcing | Stress (MPa) | | | |
|---|---|---|---|---|
| | Distance | $10^2$ km | $10^3$ km | $10^4$ km |
| Static stress changes, M8 | | $10^{-1}$ | $10^{-4}$ | $10^{-7}$ |
| Dynamic stress changes, M8 | | 3 | 0.06 | $10^{-3}$ |

Southern Tyrrhenian Sea (Italy) could be explained by the dynamic stresses imposed by a *M5.9* earthquake at ~130 km of distance, and not by the weaker static stress changes (Walter et al. 2009). Recent studies relax the importance of Coulomb stresses at long distance from the earthquake. In particular, for volcanoes within 200 km of earthquakes of $M \geq 7.5$, the eruption occurrence probability increases by ~50% for 5 years after the earthquake, likely triggered by static stress changes and/or strong ground motions. However, no significant increase in the occurrence probability of new eruptions was observed at more distant volcanoes or for smaller earthquakes (Nishimura 2017).

The fraction of eruptions that are triggered by earthquakes $X_t$ is (Manga and Brodsky 2006):

$$X_t = \frac{\Delta P_{EQ} T_V}{\Delta P_m T_{EQ}} \tag{9.2}$$

where $\Delta P_{EQ}$ is the extra pressure generated by the earthquake, $T_v$ is the ordinary recurrence time of volcanic eruptions, $T_{EQ}$ is the time between large earthquakes affecting the volcano and $\Delta P_{\mathrm{m}}$ is the overpressure required to generate tensile deviatoric stresses to nucleate and propagate a dike to the surface. The latter is estimated as 10–100 MPa for silicic magmas and less than 1 MPa for basaltic magmas (Tait et al. 1989; McLeod and Tait 1999; Jellinek and DePaolo 2003). As the static and dynamic stresses $\Delta P_{EQ}$ caused by earthquakes are typically $10^{-2}$–$10^{-1}$ MPa (Table 9.1), the overpressure $\Delta P_{\mathrm{m}}$ required to generate tensile deviatoric stresses sufficient to allow a dike to form must be within 99–99.9% of the maximum overpressure for the earthquake to initiate an eruption. Also, typical recurrence intervals $T_v$ for VEI 2 and 3 eruptions are 1–$10^2$ years, whereas the recurrence time $T_{EQ}$ for $M > 8$ earthquakes near a given volcano is $10^2$–$10^3$ years. Thus, Eq. (9.2) indicates that only a very small fraction ($\ll$1%) of eruptions will be seismically triggered at a given volcano (Manga and Brodsky 2006). This fraction likely concerns those volcanic systems already approaching the unstable state, where a stress change may anticipate a forthcoming unrest or eruption.

Viscoelastic relaxation of earthquake-induced stresses may explain not only delayed (time lag of years to decades) earthquake-earthquake triggering, but also delayed eruptions to distances of $10^3$ km (Marzocchi 2002; Marzocchi et al. 2004a). However, as the stress diffusion caused by viscoelastic relaxation results in a non-linear spatial and temporal evolution, quantifying these relationship between earthquakes and eruptions from observations remains challenging (Manga and Brodsky 2006).

Finally, in addition to earthquake-earthquake and earthquake-eruption interactions, eruption-eruption interactions between different volcanoes have been recognized. Such a volcanic coupling is largely controlled by the distance between nearby magma reservoirs, as magmatic sources that are spaced less than about 10 km apart interact, whereas those spaced more than about 25 km apart usually do not (Biggs et al. 2016). In particular, the interactions between the most closely spaced magmatic systems are controlled by the extent of shallow crystal mush layers, whereas stress changes can couple large eruptions over distances of 20–40 km, and only large dike intrusions or subduction earthquakes could generate coupled eruptions over distances of 50–100 km.

## 9.4 Understanding Unrest

Unrest may be triggered by multiple factors, acting independently or simultaneously, eventually culminating into eruption. Given the variability of the conditions leading to unrest and controlling the evolution of magmatic and hydrothermal systems, understanding what happens during unrest at a given volcano, in terms of processes and outcome, remains challenging. Nevertheless, this represents a crucial question in volcanology. In fact, understanding unrest may allow defining the conditions determining the shallow emplacement and accumulation of magma, as well as the nucleation of any feeder dike, finally providing the opportunity to better forecasting eruptions, which is the ultimate challenge for volcanology (e.g., Acocella 2014).

To determine the fate of unrest, and thus the probability of eruption, it is equally important to investigate why feeder dikes propagate (leading to eruptive unrest) or magma becomes stalled at depth (leading to non-eruptive unrest). These problems have been discussed, mainly from a theoretical perspective, in Chaps. 3 and 4. Nevertheless, studies have been also focusing on real cases concerning the propagation of feeder dikes and the stalling of magma ascending towards the surface, the latter condition also termed "failed eruption" (e.g., Crider et al. 2011; Gardine et al. 2011; Moran et al. 2011; Nishimura and Ueki 2011; Roman and Power 2011; Werner et al. 2011). In these studies on real cases, a first and common difficulty in understanding unrest and determining its fate is the general scarcity of monitoring, geophysical and geological constraints on the specific unrest episode, also to allow comparison to similar episodes. Also, even when monitoring data have been collected, a further difficulty derives from their accessibility and exploitation, as these data are often dispersed, fragmented and inhomogeneous. These limitations highlight a basic need to collect and organize data, creating large accessible databases, to understand unrest (e.g., Moran et al. 2011).

A few studies have created and investigated databases of unrest episodes (e.g., Newhall and Dzurisin 1988; Sandri et al. 2004, 2017a; Phillipson et al. 2013; Acocella et al. 2015). The description of the conditions and manifestations accompanying unrest, their statistical analysis and the identification of recurrent features provide in fact an approach to identify general behaviours, patterns, thresholds and relationships, in turn allowing to infer the possible related processes, to be understood also with the support of models (e.g., Sandri et al. 2004). In general, these studies have shown that volcanoes do not respond in the same way to unrest. The duration and outcome of unrest largely depend on the composition and size of the magmatic reservoir, which also affect the type of volcanic edifice. In particular, in the decade between 2000 and 2011 the duration of pre-eruptive unrest differed across various volcano types (Fig. 9.10; Phillipson et al. 2013). Approximately 50% of stratovolcanoes erupted after about one month of reported unrest. At large calderas this average duration of pre-eruptive unrest was about twice as long. At almost five months, shield volcanoes had a significantly longer unrest period before the onset of eruption. Also, while unrest at shield volcanoes is largely eruptive, at calderas there is a large uncertainty ($\sim$50%) on whether it culminates into eruption. In addition, calderas very frequently experience unrest, as all the calderas monitored over approximately 2 decades have shown at least one unrest episode. Therefore, despite their complexity, calderas host frequent unrest, commonly non-eruptive, and are thus ideal to observe, investigate and understand both eruptive and non-eruptive unrest processes (Acocella et al. 2015).

A few studies focused on caldera unrest. The first systematic study was a comprehensive work which included at least 1299 historical and relatively recent monitored episodes of unrest that have occurred at 138 calderas (Newhall and Dzurisin 1988). This study showed that calderas are dynamic and delicately balanced systems, which can be disturbed by even small stimuli, most notably minor tectonic strain or small-volume basaltic underplating. Different processes with different implications for hazards may

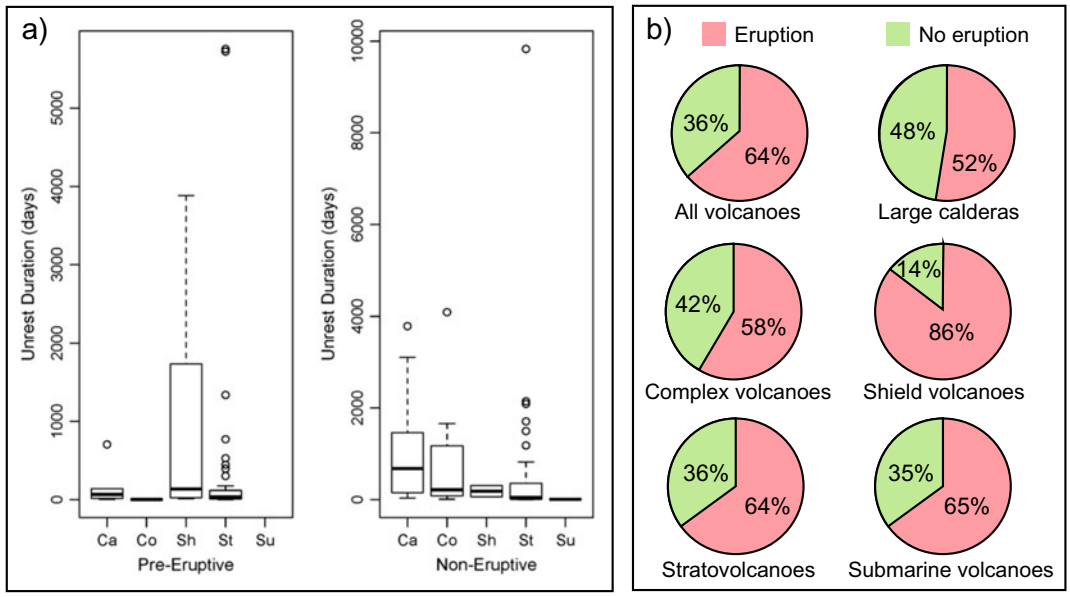


**Fig. 9.10** Unrest at volcanoes. **a** Boxplots of pre-eruptive and non-eruptive unrest duration (days), segmented by volcano type (Ca = Caldera, Co = Complex, Sh = Shield, St = Strato, Su = Submarine); note the different scales in the y axes. **b** Pie charts of the proportions of volcanoes with unrest leading and not leading to eruption (modified after Phillipson et al. 2013)

produce similar symptoms of unrest, so that even a well-understood hybrid of processes can lead to many different outcomes. This results in unrest which is likely to persist for months to years, sometimes even for decades to centuries, and to be intermittent rather than showing a systematic increase until culmination. Because of this variability, unrest alone is not a reliable indicator of impending eruption. Changes that are more diagnostic of impending eruptions are: harmonic tremor; an exponentially escalating rate of seismic energy release or a sudden, pronounced drop in seismic energy release; a sudden, pronounced increase in the uplift rate or sudden deflation after an extended period of inflation; opening of, and intense fumarolic emissions from, new fissures; or a sudden, sharp increase in hot spring discharge. Importantly, the outcome of a specific episode of unrest cannot be forecast solely on the basis of patterns of unrest at other calderas, given the uncertainties in generalizing from one caldera (or a group of) to another. When caldera unrest culminates into eruption, the latter is usually small, despite the large potential for catastrophic eruptions. Overall, this wealth of information suggests no simple solution to the interpretation and forecasting of complex events at calderas (Newhall and Dzurisin 1988).

This study has been later expanded with available monitoring data for the 1988–2014 period, providing an updated database and revealing different types of first-order behaviours depending upon the composition of the volcano (mafic or felsic) and the degree of opening of the magmatic system. The latter varies from open, through semi-plugged, to fully-plugged. In open conduits magma and gas can rise and erupt freely, whereas in semi-plugged conduits only gas can escape, and in fully-plugged (or plugged) conduits neither magma nor gas can escape (Fig. 9.11; Acocella et al. 2015). In general, unrest in mafic calderas is subtler, less pronounced and repeated, especially with open systems, which ensure a continuous, aseismic and moderate release of magma. Plugged felsic calderas are quite rare and erupt infrequently, anticipated by isolated, short and seismically active unrest. Semi-plugged felsic calderas are

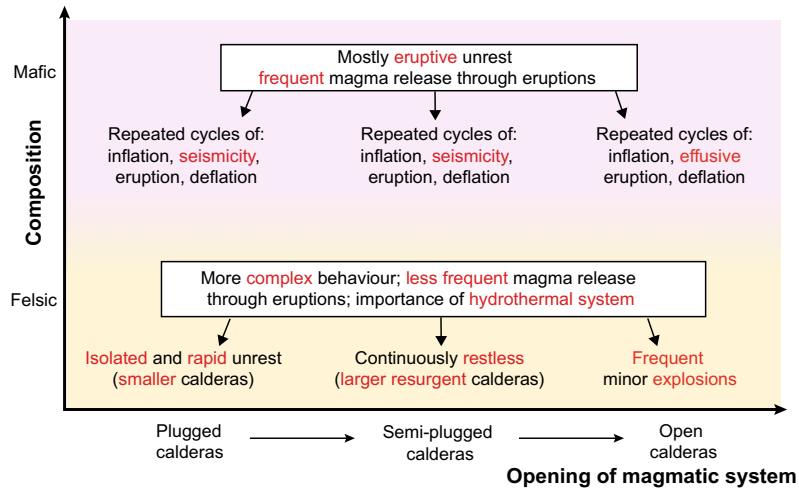


**Fig. 9.11** Types of caldera unrest as a function of the composition of the caldera (mafic vs. felsic) and the state of opening (plugged, semi-plugged, or open) of the magmatic system (modified after Acocella et al. 2015). See text for details

more common and also erupt infrequently, being often restless over decades or centuries, with uplift, seismicity and degassing and, on the longer-term, resurgence, suggesting repeated stalled intrusions. The statistical analysis of these data has highlighted some difference between eruptive and non-eruptive unrest. Eruptive unrest is shorter than non-eruptive unrest, with 72% of eruptive unrest, mainly at mafic calderas, lasting less than 10 months and showing high seismicity and degassing. The remaining 28% lasts between 10 and 18 months, with seismicity and degassing constituting a longer-duration tail (11% of the cases), or is essentially aseismic in calderas with open conduit (17%).

The limited duration of eruptive unrest (up to several months), conversely to non-eruptive unrest (up to decades) suggests that magma withstands only a limited period of "eruptibility", before becoming stored in the upper crust (Fig. 9.12; Sandri et al. 2017a). This may provide an important clue to focus research on the parameters controlling the eruptibility through time of the magma accumulated in a volcano. Preliminary studies suggest that this inferred critical period may be related to: (a) the amount of degassing of the intrusion, where higher and longer degassing reduces the volatile content of the intrusion and, at the same time, increases its cooling and viscosity (Sandri et al. 2017a); (b) the decay of the tensile stresses induced by the intrusion within the host rock, inhibiting further fracturing and magma propagation (Giudicepietro et al. 2017).

If forecasting the outcome of an isolated unrest episode is difficult, the occurrence of additional unrest episodes in the previous decades at a same volcano makes a forecast even more challenging. In fact, the intrusions emplaced in the previous unrest episodes may be activated by the last intrusion with a cumulative response, and even under a minor final

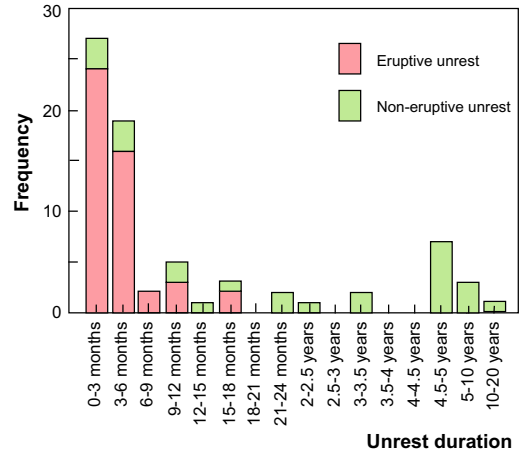


**Fig. 9.12** Histogram of the duration of unrest episodes at calderas between 1988 and 2014, considering their eruptive or non-eruptive outcome (modified after Sandri et al. 2017a)

perturbation, which alone would not have allowed the system reaching criticality. This has likely been the case of Rabaul erupting in 1994 during a minor unrest episode following a major one (Fig. 5.24b). The possibility that only a minor final perturbation leads to critical conditions with a cumulative response is particularly worrisome at restless calderas, as for example Campi Flegrei. Here the ongoing minor unrest episode (2005 to the time of writing in 2020) follows three major unrest episodes in the previous decades that may have promoted thermal weakening of the caldera, raising concern for hazard assessment and risk mitigation. A similar multiple disturbance over decades to months before eruptions has been recognized at Santorini before the ~1600 BC major eruption (Fig. 5.14a; Druitt et al. 2012; Chiodini et al. 2016).

While the unrest phase may help in understanding the state of the volcano and forecasting any impeding eruption, any estimate of the size of a possible eruption currently remains purely speculative, possibly even in the end-member case of super-eruptions. In fact, what is known about super-eruptions, in terms of physical processes, represents a logical extension of the activity observed and inferred from smaller eruptions of the same composition, the only difference consisting of the volume of released magma. This implies that there are no grounds for supposing that super-eruptions involve novel processes, and thus unrest behaviours, that do not also apply to other eruptions (Wilson 2008).

In addition to isolated studies providing and analysing databases, important international initiatives are managing more comprehensive databases. These include WOVODAT (https://www.wovodat.org/), which aims at collecting homogeneous monitoring data on volcanoes from a constellation of volcano observatories worldwide (with data from > 900 unrest episodes covering > 75 volcanoes already accessible; Newhall et al. 2017), and Geohazards Supersites (https://geo-gsnl.org/supersites/permanent-supersites/), developed to encourage scientific exploration of earthquake and volcano hazards to improve disaster risk management at specific sites around the globe.

## 9.5 Assessing Volcanic Hazard and Forecasting Eruptions

As introduced in Sect. 1.10, volcanic risk is defined as the product of volcanic hazard, exposure and vulnerability. Volcanic hazard is the competence of volcanologists, who are in charge of studying and monitoring volcanoes, to define their state, define and forecast any hazard and communicate their warnings to civil defence, authorities and public. The definition and reduction of exposure and vulnerability is the competence of experts with complementary knowledge (engineers, architects, urban planners, modellers, doctors) and, most importantly, authorities (including civil defence), whose duty is to manage a crisis with appropriate mitigation procedures (e.g., Tilling 1989). Therefore, volcanologists are required to provide appropriate hazard assessment, largely in collaboration with civil defence and authorities, to mitigate risk. In practical terms, this includes the definition of hazardous scenarios (including the reference eruption), the establishment of early warning systems, the definition of volcano alert levels and the capability to forecast eruptions.

**Hazardous scenarios** are expected hazardous events that may occur at a certain volcano, based on its current state. Defining hazardous scenarios is helpful for civil defence and authorities to take actions and mitigate the related risks. A volcano may be the source of very different types of hazards, directly triggered by volcanic activity (as pyroclastic flows, ash fall, lava flows, debris avalanches, surface deformation, degassing, seismicity) or indirectly triggered (as lahars, floods, tsunami, acid rain, famine, diseases, climate change), manifesting at different times from the onset of an eruption and impacting areas at various distances. These hazards are often related to each other, so that the manifestation of a specific hazard may trigger another hazard, amplifying the impact, in a **multi-hazard** combination. Multi-hazards should be adequately investigated establishing the ranking of the different types of hazard and taking into account for their possible interactions (Marzocchi et al.

2012). Multi-hazard assessment may be supported by a **conceptual model**, which consists of a theoretical frame based on any type of first-order evidence that describes the general evolution of a volcano in a reference period. In order to be useful, the conceptual model has to be kept as simple as possible, with its main constituents being shared by the wider scientific community. An example of volcano involving a potential chain of multi-hazards is Ischia island (Italy), characterized by notable resurgence (~1000 m of uplift in the last ~35 ka) associated with widespread gravitational instability, minor eruptions outside the resurgent block and recurrent seismicity along a border of the block (De Vita et al. 2010; Trasatti et al. 2019). Here a multi-hazard assessment has relied on a conceptual model, valid for the last ~10 ka, based on the general understanding of the behaviour of a magmatic system experiencing resurgence. This conceptual model has allowed zonation of the origin of the different hazards, as well as the related hazardous scenarios (for eruptions, seismicity, landslides, tsunamis), also integrated in a multi-hazard perspective (Fig. 9.13; Galetto et al. 2017; Selva et al. 2019).

In high-risk volcanoes a reference eruptive scenario should be considered. The **reference eruption** allows civil defence and authorities to prepare appropriate mitigation procedures and emergency plans, so that established and effective protocols may be used in case of impending eruption. The reference eruption should meet a balance between likelihood and severity and should correspond to a reasonable evaluation of the "acceptable risk", as based on probabilistic studies. For example, the reference eruption for Vesuvio (Italy) has been evaluated considering the past eruptive history of the volcano (mainly consisting of violent Strombolian VEI 3 eruptions, sub-Plinian VEI 4 eruptions and Plinian VEI 5 eruptions), as well as their conditional (conditioned to the occurrence of an eruption) probabilities in a time frame of 200 years. Accordingly, the probability of a VEI 3 eruption is the highest (72%), whereas the

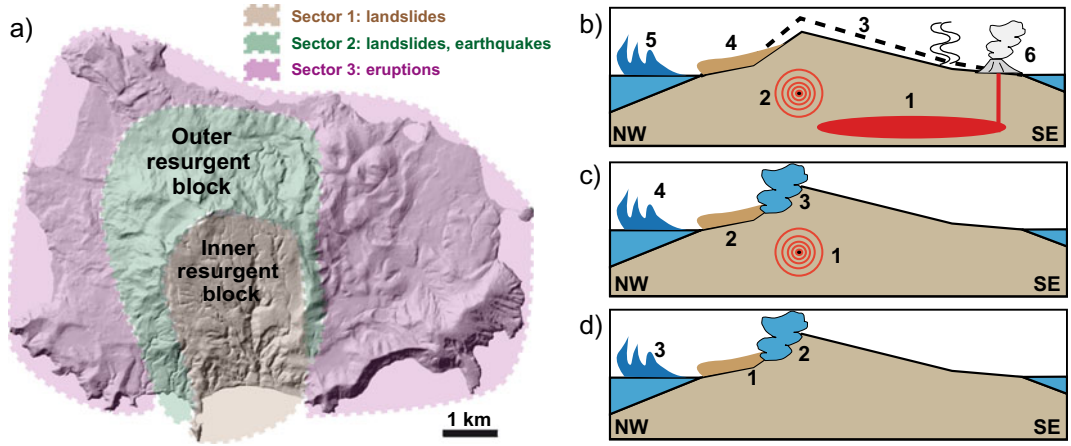


**Fig. 9.13** Example of multi-hazard approach at Ischia (Italy; modified after Selva et al. 2019). **a** Schematic view of the areas source of the main hazards; dashed boundaries are meant to represent broad transitions zones. **b**–**d** NW–SE section views through the resurgent block illustrating the possible multi-hazard scenarios; not to scale. **b** Magma-induced multi-hazard: the emplacement of a shallow intrusion (1) induces seismicity (2) and deformation (3), possibly destabilizing the resurgence border (4) and, in case the landslide products enter the sea, triggering a tsunami (5); eventually, the intruded magma may erupt (6). **c** Seismicity-induced multi-hazard: an earthquake (1) may trigger the collapse along the resurgent block (2), eventually promoting phreatic eruptions through decompression (3) and, if the collapsed deposits enter the sea, triggering a tsunami (4). **d** Landslide induced multi-hazard: collapse along the border of the resurgent block (1) may promote phreatic eruptions through decompression (2) and, if the collapsed deposits enter the sea, may trigger a tsunami (3)

**Table 9.2** Conditional probabilities for expected eruptions with different size at Vesuvio (Italy) for time frames between the next 60 and 200 years and from 60 years onward (modified after Marzocchi et al. 2004b)

| Eruptive activity | VEI | Conditional probability (%) | |
|---|---|---|---|
| | | (>60 to <200 years) | (>60 years) |
| Violent Strombolian | 3 | 72 | 65 |
| Sub-Plinian | 4 | 27 | 24 |
| Plinian | 5 | 1 | 11 |

probability of a VEI 4 eruption is lower, but not negligible (27%) and the probability of a VEI 5 eruption is much smaller (1%) (Table 9.2; Marzocchi et al. 2004b). Choosing a VEI 3 as the reference eruption considers the most likely eruptive event, but neglects a still relatively probable VEI 4 eruption. Choosing a VEI 4 as the reference eruption allows to include a VEI 3 event and to be on a safer side including a relatively probable VEI 4 eruption. Choosing a VEI 5 eruption brings to an even safer approach, but requires much more demanding mitigation measures for an unlikely event. Based on these considerations, the reference eruption for Vesuvio has been taken as a VEI 4 sub-Plinian eruption. This leaves out an unlikely VEI 5 Plinian eruption as the **acceptable risk** that a community is willing to take considering the benefits and costs (including feasibility) of risk mitigation. Therefore, a reference scenario is neither necessarily the most likely nor the most hazardous event, its choice resulting from a trade-off between size, probability of occurrence and acceptable risk. Note that the acceptable risk is usually not defined by the volcanological community, as requiring knowledge on the expected impact of a hazardous event and the capability of a community to face it. Recent hazard studies go beyond the concept of eruptive scenario, to take into account for full variability of events in addition to a specific size class (Sandri et al. 2016).

An **Early Warning System** (EWS) is used by volcanologists to inform authorities about the occurrence of any impending hazard. It consists of capacities to generate timely warning information to enable those threatened by a hazard to prepare and act to reduce harm or loss. An EWS is released by volcano observatories and concerns information that often describes the state of a volcano, the expected hazards, a time frame for specific activity and generic recommendations (Gregg et al. 2015). This information is disseminated to agencies linked to emergency management/civil defence, aviation, media and the public. EWSs are a key risk reduction tool as part of a programme of volcanic hazard assessment that brings together the physical and social sciences to enable effective decision-making.

A **Volcano Alert Level** system (VAL) is a specific key tool or subsystem of a volcano EWS that simplifies the communication of volcanologists' interpretation of data (Newhall 2000). A VAL consists of a series of levels that correspond to increasing stages of volcanic unrest. Ideally, the VAL should increase progressively before eruption or increase and then decrease where unrest does not proceed to eruption (Table 9.3; Winson et al. 2014). Most VALs are country-specific and, although based on different schemes, include a quick description of the activity occurring at a volcano, with indication of the potential time frame before an event, and a colour scale to communicate an escalating (or decreasing) volcanic hazard. Colours are in the "traffic light" scheme, where green is equated with normal conditions and red is the most dangerous level (usually an impending eruption). These features respond to the original meaning and issuance of the VALs, which date back to the late 1980s and were aimed at defining the state of a volcano, although implying forecast windows used by officials to decide on mitigation actions. In the last decades, some VALs have included recommended actions, as information on exclusion zones and **evacuation**, that is the temporary

**Table 9.3** Example of alert levels used for the 1991 Pinatubo (Philippines) crisis; colours allow linking alert levels to mitigation measures (modified after Newhall 2000)

| *Alert level* | *Criteria* | *Interpretation* |
|---|---|---|
| No alert | *Background*; quiet | No eruption in foreseeable future |
| Level 1 | *Low level* seismicity; other unrest | Magmatic, tetonic, or hydrothermal disturbance; no eruption imminent |
| Level 2 (May 13) | *Moderate level* of seismicity, other unrest, with positive evidence for involvement of magma | Probable magmatic intrusion; could eventually lead to an eruption |
| Level 3 (June 5) | *Relatively high and increasing unrest* including numerous b-type earthquakes, accelerating ground deformation, increased vigor of fumaroles, gas emissions | If trend of increasing unrest continues, eruption possible within 2 weeks |
| Level 4 (June 7) | *Intense unrest*, including harmonic tremor and (or) many "long-period" (low-frequency) earthquakes | Eruption possible within 24 hours |
| Level 5 (June 9) | *Eruption in progress* | Eruption in progress |
| | (Note that large-scale explosive eruptions began June 12; climactic eruption occurred on June 15) | |

*Mitigation measures as a function of alert level*

10,000 evacuated on June 5

25,000 evacuated on June 9 (20 km zone)

40,000 evacuated on June 10

85,000 evacuated on June 14 (40 km zone)

transfer of the potentially affected population. This extension of the original concept of VAL has brought to some uncertainty on whether volcanologists should be the de facto decision makers or not, with an assumption of responsibility that may go beyond the expertise of the scientist and which, in most countries, is not granted by a corresponding societal mandate (Papale 2017). Despite this, VALs remain a useful communication tool to codify the state of a volcano during unrest, and their changes at volcanoes experiencing unrest have been also used to track the response of volcanologists during volcanic crises (Fig. 9.14; Winson et al. 2014). In particular, only 19% of the VALs issued between 1990 and 2013 for 194 events that ended with eruption accurately reflect the hazard before eruption. This increases to ~30% considering eruptions with VEI $\geq$ 3, with VALs of eruptions from closed conduit volcanoes more appropriately issued than those from open conduits. Considering also the alerts for unrest without eruption (in the 30 days following the change in the VAL) the number of accurate VALs increases from 19 to 55%. These results show that the forecasting capability of the volcanological community is still far from being optimal, with a substantial number of "missed" (onset of eruption not preceded by increase in the VAL) and "too late" (VAL increased for the first time after the eruption began) change of alert levels, while the "premature" changes (VAL increased but subsequently decreased to lower levels prior to the onset of eruption changes) remain low. Both the "missed" and the "too late" cases imply a **missed alarm** for evacuation before eruption: missed alarms can easily lead to tragedy. "Premature" changes in VAL may be also problematic, as potentially leading to a **false alarm** for evacuation, which undermines trust in scientists and authorities. Quite surprisingly, the success rate for all alerts (with or without eruption) is only moderately improving over time, suggesting that the implementation of monitoring systems and our enhanced understanding of volcanoes have carried limited benefits so far. In facing a volcanic crisis, an additional useful tool is the cost–benefit analysis. This, based on the forecast of a certain event (made by volcanologists), allows decision makers to assess the costs and possible benefits of specific mitigating actions (e.g., Marzocchi and Woo 2007).

**Eruption forecast** is the capability to anticipate the occurrence of an eruption in order to provide the possibility to take appropriate mitigation measures, most commonly to evacuate the area potentially affected by the eruption. Eruption forecast is probably the ultimate challenge

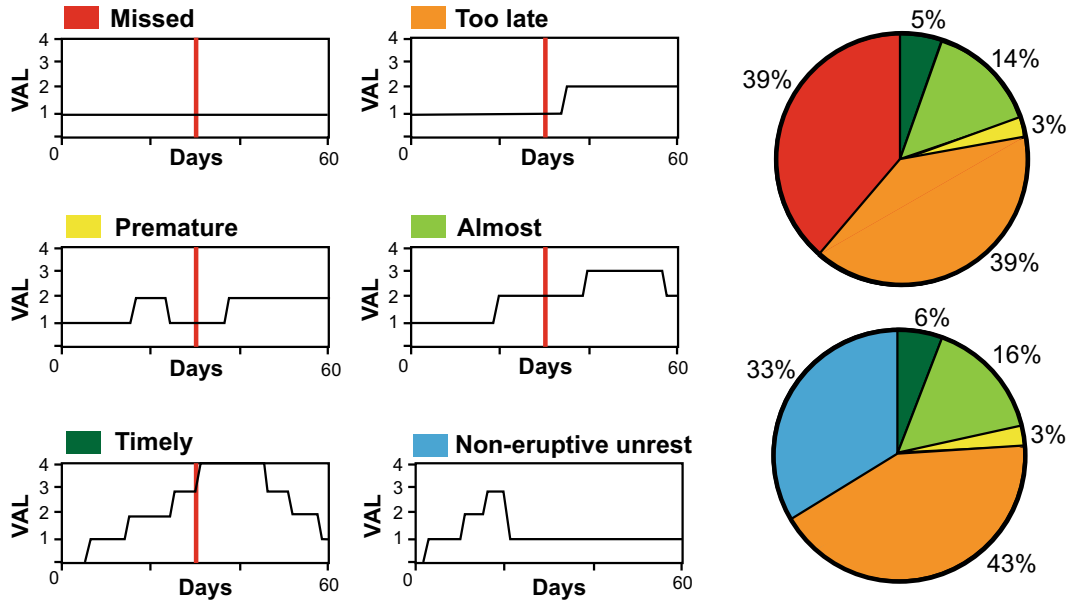


**Fig. 9.14** Left diagrams: classification of the issued alert levels relative to eruptions for 194 events that have occurred between 1990 and 2013. The VALs are plotted against time and the red line denotes the onset of the eruption. Right diagrams: pie charts showing the proportion of the issued alert levels relative to eruptions in eruptive unrest episodes (top) and including non-eruptive unrest as a percentage of all cases except "missed" (bottom; modified after Winson et al. 2014)

for volcanologists, in which all the knowledge acquired on volcanic and magmatic processes is directed towards the benefit of society. Similarly important is also forecasting what happens after the eruption onset, for example if an eruption may consist of multiple phases defined by different styles of activity (e.g., effusive and/or explosive) and/or quiescent periods between them (Bebbington and Jenkins 2019). In the last decades there has been a variable preparedness and capability of the volcanological community to forecast impending eruptions. Some eruptions have been successfully forecast, while others not. This has led to successful evacuations of the potentially affected population, failed evacuations (no eruption occurred) or missed evacuations (eruptions have occurred before). As a result, volcanology has experienced successes and confidence, as well as disasters and frustrations, in forecasting eruptions.

Successful forecasts have been made at Mount St. Helens in 1980 and Pinatubo in 1991. Both stratovolcanoes passed from a centuries-long quiescence to unrest, characterized by the progressive increase in the intensity of the monitoring signals and occurrence of phreatic eruptions, leading to eruption within just 2–3 months. At Mount St. Helens the emplacement of a cryptodome within the edifice produced the bulging of ~100 m of the northern flank, which evolved in sector collapse triggering a lateral eruptive blast in May 1980. Several eruptions between June 1980 and December 1982 were also successfully forecast, mainly using seismicity and deformation data (see Sect. 6.8.2; Lipman and Mullineaux 1981; Swanson et al. 1983). At Pinatubo the magma intruded below the edifice, probably following a nearby *M7.8* regional earthquake. The gradual increase in activity during unrest (increased and shallowing seismicity, increased $SO_2$ emissions and phreatic eruptions) called for the evacuation of progressively wider areas until the day before the eruption climax (Fig. 9.15; Newhall and Punongbayan 1996). Despite the large size of the eruptions (VEI 5 for Mount St. Helens and 6 for Pinatubo), the successful forecasts and

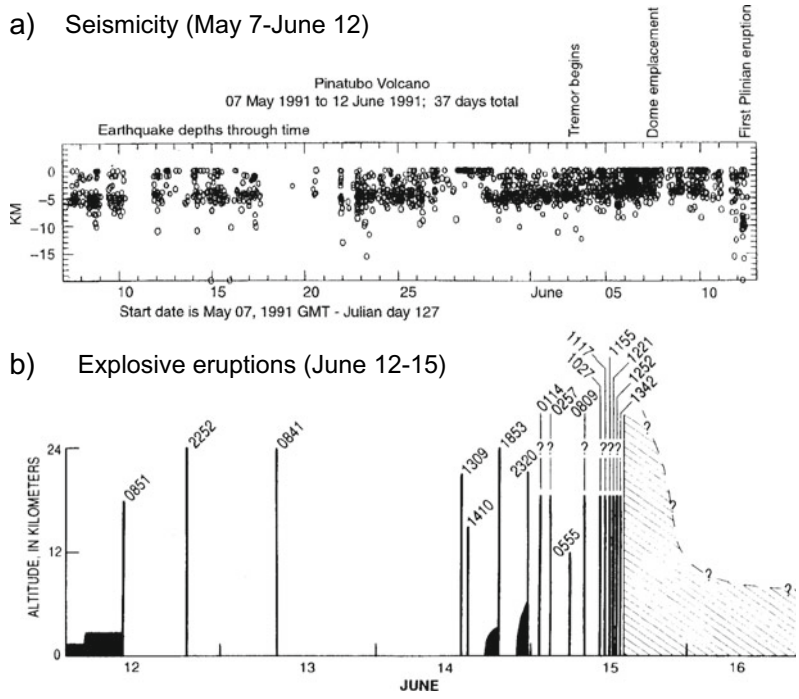


**Fig. 9.15** Pre-eruptive and eruptive events associated with the 1991 Pinatubo (Philippines) eruption, the largest in decades. **a** Earthquake depths from May 7 to June 12, 1991; data gaps occurred on May 10–11, 17–19, and 21–22. **b** Chronology of explosive eruptions and related maximum altitude in June 12–15; four-digit number is local time of eruption onset; emission indicated by diagonal pattern is schematic (McNutt 2000)

evacuations limited the death toll to 57 victims at Mount St. Helens and 847 (mostly for measles in the evacuation camps) at the much more densely inhabited Pinatubo.

Volcanology has also witnessed disasters in recent times, as in 1985 at Nevado del Ruiz (Colombia), where unrest was characterized by the progressive increase in the seismicity, degassing and phreatic activity for nearly one year, culminating in a magmatic eruption in November. This eruption melted the ice on the volcano summit, producing lahars travelling at 60 km/hr within the valleys around the volcano, one of which hit the ~60 km distant village of Armero, causing ~23,000 victims. While the potential hazard deriving from lahars was foreseen by volcanologists months in advance, failure to take actions before and during the eruption in a wider context of improper management resulted in tragedy, despite the minor size of the VEI 3 eruption, emitting only $5 \times 10^6$ $m^3$ of magma (Barberi et al. 1990; Voight 1990).

In other situations, the response of scientists and authorities to a volcanic crisis may be considered premature, at least in retrospective. This is the case of La Soufriere volcano (Guadeloupe, Antilles) in 1976, where an explosion in July marked the onset of nine months of emission of $10^6$ $m^3$ of non-juvenile tephra. An increase in the VT seismicity in August called for a contentious evacuation, not agreed on by all the scientists, of 74,000 people in less than 24 h. The evacuation ended in December, following the decrease in the intensity of the monitored signals. The 4-months long evacuation of 74,000 people made this crisis one of the most costly of twentieth century, although without loss of life, causing severe socio-economical difficulties on the island. Later understanding allowed defining the crisis as resulting from an aborted magmatic episode, with the unrest signals produced by the migration of magmatic gases into the hydrothermal system. These gases dissipated heat, inhibited magmatic eruption and promoted phreatic eruptions (Hincks et al. 2014).

Even an early alarm may cause difficulties to volcanologists, authorities and population; this is the case of the 2017 Agung (Bali, Indonesia)

eruption, which was preceded by 5 months of unrest. An early increase in seismicity prompted the evacuation of 140,000 people (including 70,000 who spontaneously evacuated) for one month at 2 months before the onset of the eruption. The delay between intense unrest and eruption caused considerable challenges to emergency responders, local and national governmental agencies, and population near the volcano (Fig. 9.16; Syahbana et al. 2019).

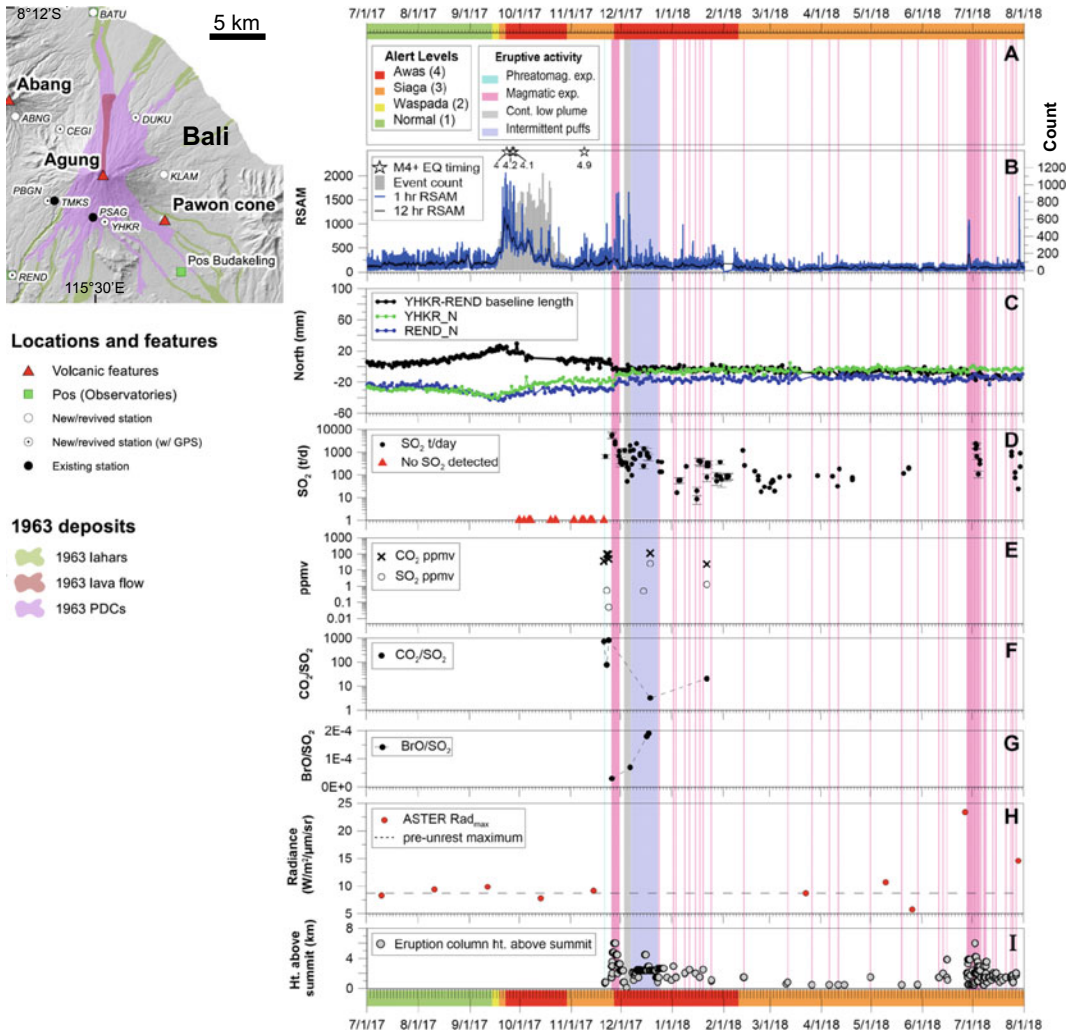


**Fig. 9.16** Timeline of the 2017–2018 unrest and eruption at Mount Agung (Bali, Indonesia, shown in left inset). **a** Alert level changes. **b** Real-time Seismic-Amplitude Measurement (RSAM) from TMKS, and daily seismic event counts. $M \geq 4$ earthquakes displayed as stars. **c** GNSS displacements and baseline length between YHKR and REND. **d** $SO_2$ emission rates from ground-based mobile DOAS. **e** $CO_2$ and $SO_2$ mixing ratios from drone-transported Multi-GAS. **f** $CO_2/SO_2$ ratios (molar) from Multi-GAS. **g** $BrO/SO_2$ ratio from mobile DOAS. **h** Advanced spaceborne thermal emission and reflection Radiometer (ASTER) maximum radiance values from the crater, with pre-unrest maximum radiance plotted as dashed line. **l** Eruption column heights. Running across the entire graph are phreatomagmatic (blue) and magmatic (pink) explosions, periods of continuous ash venting (grey) and intermittent ash puffing (purple; modified after Syahbana et al. 2019)

These representative cases show how forecasting eruptions in the recent past has brought to very different outcomes, which may depend on several features. Among these are the different degree of knowledge and consciousness of the state of a volcano and its processes, as derived from geology and monitoring data, and the experience of the scientific community involved. The pre-eruptive behaviour of the volcano may also show very different features. For example, unrest characterized by the progressive increase of the monitoring signals is more "predictable" (Mount St. Helens in 1980 and Pinatubo in 1991). Conversely, unrest showing a significant decrease in the monitoring signals anticipating eruption leads to non-linear behaviours that are more difficult to interpret (Rabaul before 1994 and Agung in 2018). Also, in some cases, possible **precursors,** or specific anomalies that may anticipate an eruption within a certain time frame, may be recognized and used for forecast, while in other cases this is not possible. With this regard, it should be made clear that it is currently extremely difficult to identify eruptive precursors. This difficulty mainly results from the limited knowledge and measurement of the parameters potentially controlling an impending eruption, which may depend on the magma properties (as the viscosity, density, gas content, crystallization and excess pressure), the host rock properties (as the stress state around the magma chamber), and external processes affecting the response of a system in a nearly critical state (as regional seismicity and rainfall; e.g., Chiodini et al. 2016; Albright et al. 2019; Farquharson and Amelung 2020; Manga 2020). The identification of promising eruptive precursors has been limited to specific (largely open conduit) volcanoes with frequent and regular eruptive behaviour, as Mount St. Helens between 1980 and 1982 (Swanson et al. 1983) or Mount Etna. At Etna, an infrasound array has been detecting explosive eruptions in the last decade, generating an automated pre-alert with a 97% of success rate (Ripepe et al. 2018). While providing the first case of automatic operational early warning system, and finding potential application also to other volcanoes, this precursors based approach remains limited to open conduit volcanoes characterized by lava fountaining. Several recent approaches rely on the use of artificial intelligence to more accurately monitor and eventually forecast eruptions, from using algorithms to initially sort through the huge amount of available space monitoring data and then focus on the volcanoes of most interest, to developing systems able to detect potential signs of unrest automatically. While the current aim of these efforts is to process all available monitoring data of volcanoes, a longer-term perspective may allow issuing warnings of volcanic activity on societally relevant time frames, although eruption forecasts are not expected to be reliable as weather forecasts (Gaddes et al. 2018; Albino et al. 2019; Witze 2019; Palmer 2020; Poland and Anderson 2020).

Despite any rare case limited to favourable conditions, currently there is no unique and reliable eruptive precursor in volcanology, and the forecasting capability still largely results from the non-unique interpretation of multi-parametric data. As anticipated in Sect. 9.2, the most reliable indicators of an impending eruption in closed conduit volcanoes remain the multi-parametric data allowing detection of a dike propagating from a zone of shallow magma accumulation towards the surface. Notwithstanding this possibility, as mentioned, there is still no reliable precursor to infer the size of an impending eruption. Phreatic eruptions are possibly even harder to forecast, even if the volcano is thoroughly monitored, as not being anticipated by dike propagation and with any unrest phase showing extremely variable duration, from minutes to years, with subtle variations in the monitoring parameters (e.g., Kato et al. 2015; Caudron et al. 2019).

In forecasting eruptions it is essential to refer to the **time window** of the forecast. This is mainly determined by the time span and resolution of the available data, as a forecast can look no farther forward than the time span of data on which it is based, nor can it have any greater resolution than that of the data on which it is based. A geologic record of millennia and resolution of centuries applies to coming centuries

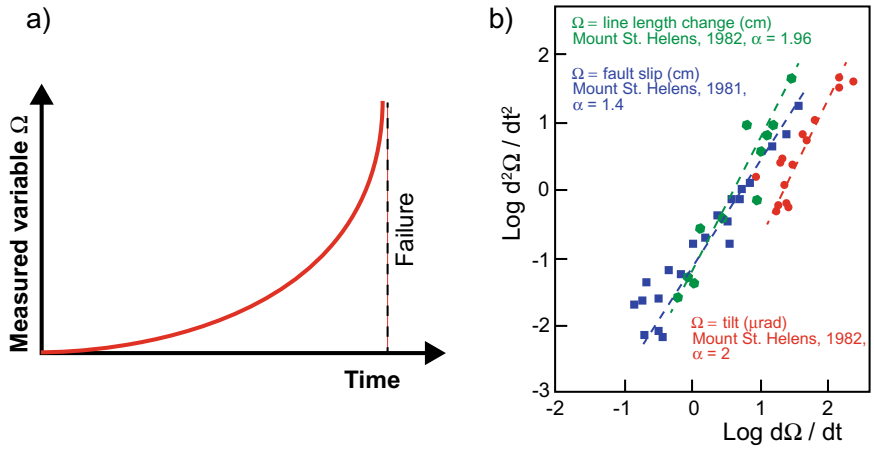


**Fig. 9.17** **a** Principle of the Failure Forecast Method, where a measured variable Ω increases approaching failure: in this case an exponential increase is shown. **b** Application to erupting volcanoes: the diagram shows the log–log relationship between the acceleration of the monitored variable Ω and its rate for three eruptions at Mount St. Helens, in which Ω consists of different deformation parameters (modified after Voight 1988)

and millennia, and a record of last week's monitoring applies to next week. Therefore, forecasting eruptions at quiescent volcanoes relies on the knowledge of the past eruptive frequency and size of the volcano, requiring a longer-term time window, from years to centuries. Conversely, forecasting eruptions during ongoing unrest relies on the knowledge of the recent variation of the monitoring parameters, requiring a shorter time window, from days to months. Eruption forecast has moved from a deterministic (focused on the short-term) towards a probabilistic (concerning both the long- and short-term) approach, both illustrated below.

## 9.6 Deterministic Forecasting

**Deterministic eruption forecasting** is based on the notion that an eruption can be satisfactorily predicted in time and space. The deterministic approach was popular at the end of the last century, following the successful management of the 1980 Mount St. Helens and 1991 Pinatubo eruptions. The progression of the activity observed in both pre-eruptive periods highlighted a linear behaviour, giving volcanologists the confidence that eruptions could be predicted ahead of a few days-weeks. The deterministic approach considers that, in analogy to what observed during the deformation of a specimen in a laboratory test, the volcanic system undergoes progressive mechanical failure until reaching rupture, that is when eruption occurs (Fig. 9.17a). This progressive failure may be recognized through monitoring data mainly for short-term predictions, although decade-long time-series of monitoring data may be also used.

The theoretical rationale of this approach, known as the **Failure Forecast Method** (FFM), is summarized by the equation which links the acceleration of any physical (or even chemical) measured variable Ω to its rate, as:

$$\frac{d^2\Omega}{dt^2} = K\left(\frac{d\Omega}{dt}\right)^{\alpha} \tag{9.3}$$

where, $K$ and $\alpha$ are constants and $t$ is the time (Voight 1988; Voight and Cornelius 1991). In particular, $\alpha$ (with $1 \leq \alpha \leq 2$) controls the type of acceleration involved: $\alpha = 1$ corresponds to an exponential increase, whereas $\alpha = 2$ to a hyperbolic increase. As the rate of the variable increases, the acceleration becomes larger and increases the rate more quickly than before. The deterministic forecasting potential of this relation depends on estimating the time at which the rate tends to infinity, that is the failure, or eruption. In

the general case that $\alpha \neq 1$, solutions to Eq. (9.3) take the form of a power law increase in the rate of the monitored variable with time:

$$\frac{d\Omega}{dt} = j(t_f - t)^{-p} \tag{9.4}$$

where $t_f$ is the time of failure, $j$ is a multiplicative amplitude term and $p = 1/(\alpha - 1)$ is a power law exponent. Values of $j$ and $\alpha$ may be empirically estimated from a plot, such as that in Fig. 9.17b. The accuracy of this approach is determined by the precision and frequency of observations and the regularity and continuity of the observed process. Equation (9.4) can be solved by linearizing the problem in the form:

$$\left(\frac{d\Omega}{dt}\right)^{\frac{-1}{p}} = j^{\frac{-1}{p}}(t_f - t) \tag{9.5}$$

and using standard least squares regression to determine the failure time (Voight 1988). Commonly $p \sim 1$ (Kilburn 2003), in which case the solution is a straightforward regression of inverse rate against time. The time of failure can be best ascertained graphically by extrapolation of the concave curve $(d\Omega/dt)^{-1}$ versus time to a predetermined intercept. In fact, forecast accuracy is aided by inverse representation, as large differences and trends in such sequences may be recognized earlier (Voight 1988).

While having raised hopes of making deterministic and objective forecasts of eruptions and having provided clues to developing a formal physical model, this simple approach presents several limitations. First, the method is not quantitatively linked to a physical process, as it reveals preferred types of acceleration in whatever is the controlling process (Eq. 9.3). Second, the best-fit trends for individual time series of FFM are not unique and statistical fits can yield ambiguous results. Also, since a week or more is required to identify an accelerating trend, any forecast is unlikely to be reliable more than a few days at most in advance (Kilburn and Sammonds 2005). In addition, closed conduit volcanoes and rock physics experiments show that rates of fracturing can accelerate while the deformation rate remains constant. Under such conditions, Eq. (9.3) may accommodate a seismicity rate, but not the contemporaneous rate of deformation, so describing only part of the precursory processes that lead to eruption (Kilburn 2018).

These limitations have brought to the modification of the FFM or the formulation of other deterministic approaches (Bell et al. 2011; Robertson and Kilburn 2016; Kilburn 2018). Among these, a modified physical model (known as the **parent model**) shows that precursory time series are governed by a parent relation between seismicity and deformation. This relation postulates that, in the failure of a material, the applied differential stress increases from zero and the deformation evolves from the elastic, through quasi-elastic to inelastic regimes (Fig. 9.18; Kilburn et al. 2017; Kilburn 2018). The start of the inelastic regime coincides with deformation under a constant maintained stress. Here the deviation from elastic behaviour is caused by faulting, and faulting may be expressed by the cumulative number of volcano-tectonic (VT) seismic event. The number of VT events increases exponentially with deformation in the quasi-elastic regime, but linearly with deformation in the inelastic regime. This theoretical model has been applied to pre-eruptive seismicity-deformation sequences from different volcanoes, where the monitoring data confirmed the expected evolution from quasi-elastic to inelastic behaviour, with eruption appearing within the inelastic domain. This occurs independent of the type of volcano, the duration of precursor, magma composition and style of eruption. Therefore, the parent model may provide a tool to predict eruption based only on the seismicity and deformation patterns. This model also underlines the importance of considering the cumulative, even if non-linear, unrest history at a certain volcano, rather than the isolated unrest events, as highlighted in Sect. 8.3.3 comparing the recent unrest episodes at Rabaul and Campi Flegrei. In particular, the cumulative seismicity-deformation from consecutive unrest episodes indicates that the inelastic threshold was reached at Rabaul just before the eruption. Conversely, at Campi Flegrei, experiencing a partial recovery of the deformation after the major uplift of 1982–1984,

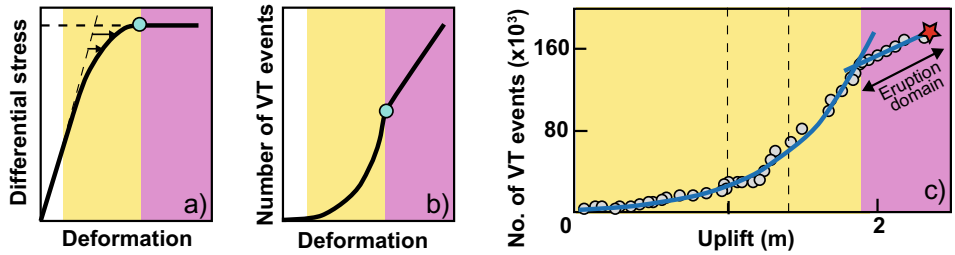


**Fig. 9.18** Theory of the parent model illustrating the relation between elastic deformation and faulting (modified after Kilburn et al. 2017). **a** In the failure of a material, the applied differential stress increases from zero and the deformation deviates from the elastic (white), through quasi-elastic (yellow) to inelastic (purple) regimes; blue dot shows onset of inelastic regime under a constant maintained stress. **b** The deviation from elastic behaviour is caused by faulting, here expressed through the cumulative number of volcano-tectonic (VT) earthquakes. The number of VT events increases exponentially with deformation in the quasi-elastic regime, but linearly with deformation in the inelastic regime, where eruption is expected. **c** The evolution from quasi-elastic to inelastic deformation was observed (blue curve and line fitting data from grey dots) during the 23-year unrest before the 1994 eruption at Rabaul caldera (Papua New Guinea); red square denotes eruption, black dashed lines refer to the 1983–1985 episode of accelerated uplift

the inelastic threshold has not been achieved yet (Kilburn et al. 2017). These results also suggest that the FFM is a particular form of the parent model when rates of stress supply are constant. The outcome of the parent method yields deterministic criteria that can be incorporated into existing operational procedures for evaluating the probability of crustal failure at closed volcanoes. This model, however, is still an incomplete description of pre-eruptive conditions at volcanoes. It identifies conditions for bulk failure in the crust, which, although necessary to open a new pathway for magma ascent, do not guarantee that magma reaches the surface. Also, magma may reach the surface soon after the inelastic behaviour is reached (as at Kilauea, Hawaii, in 1971–1972) or with some further delay (as at El Hierro in 2011), thus adding uncertainty in the prediction. The parent model thus provides a promising starting platform for identifying additional precursory trends and pre-eruptive criteria through a deterministic approach (Kilburn 2018).

## 9.7 Probabilistic Forecasting

While some unrest episodes show a progressive increase in the intensity of the monitoring signals, culminating in eruption, as at Pinatubo in 1991, many other unrest episodes show more complex and **non-linear** behaviour, in which the variation of the output is not proportional to the variation of the input (Tilling 1988). In general, this behaviour results from the fact that material failure is typically non-linear and volcanoes are highly complex systems hosting a wide range of kinetic and dynamic magmatic processes, governed by many degrees of freedom at the same time, and leading to a wide range of potential behaviours intrinsically unpredictable. This condition is complicated by the limited access to and capability of understanding and quantifying these processes, which are also accompanied by intrinsic uncertainties that may be quantified and reduced, but cannot be completely removed. In fact, natural processes usually own a scientific uncertainty (**epistemic uncertainty**), due to the availability of limited data and limited understanding, which may be in principle reduced, and an irreducible unpredictability intrinsic in the system (**aleatory uncertainty**), which cannot be eliminated (Marzocchi and Bebbington 2012). Due to the uncertainties and the complexity of non-linear systems, a deterministic prediction of eruptions is, in most cases, not achievable. Rather, in the last two decades there has been a shift towards probabilistic forecast of eruptions that takes also into account for uncertainties (e.g., Sparks 2003; Sparks and Aspinall 2004). In forecasting volcanic hazards and assessing risks,

one needs to estimate the probability that a hazardous event will happen, the probability that the event will affect a particular place and the probability that the effects will include fatalities and property damage.

In general, there are two main classes of probability: the frequentist (objective probability) and the degree of belief (subjective probability). The **frequentist** approach views probability as the long-run expected frequency of occurrence, with the probability $P$ of occurrence of an event $A$ being:

$$P(A) = n/N \tag{9.6}$$

where $n$ is the number of times the event $A$ occurs in $N$ opportunities. An estimate of objective probability can be obtained through a stochastic model or empirical analysis of frequencies in datasets. **Stochastic** models possess some inherent randomness (the same set of parameter values and initial conditions will lead to an ensemble of different outputs) and are widely used in long-term eruption forecast, where the primary information comes from historical and geological catalogues of eruption onsets and, in some cases, sizes. Stochastic models can also take into account for a **multivariate analysis**, which involves observation and analysis of more than one statistical variable at a time (Jaquet et al. 2006; Bebbington 2009; Marzocchi and Bebbington 2012). In this context, eruptions are considered as the outcome of stochastic point processes. This approach simply calculates the frequency of past events, assuming that this frequency is an estimator of the true, and unknown, probability for the future events. This analysis implies the absence of a reference model, and faithfully reproduces the random variation from the catalogue in forecasts. Unless the catalogue is a large one, which is unlikely in volcanology, the resulting forecasts tend not to be smooth and can be biased (Marzocchi and Bebbington 2012).

The **degree of belief** is a level of confidence or credence that expresses in statistical terms how much a person, or a group, believes that a proposition is true: its use is commonly required in the case of a limited amount of data. The degree of belief is at the base of subjectivist, or **Bayesian,** probability in which, rather than a "true" probability to estimate, any quantity is expressed by a probability distribution. This perspective can be directly linked to the aleatory uncertainty (described by a "best-guess" value of the distribution, such as the mean or the median) and epistemic uncertainty (described by the dispersion around the best-guess in the probability distribution). The probabilities are combined through Bayes' theorem, which is a formula that describes how to update the probabilities of hypotheses when given evidence, following from the axioms of conditional probability, that is the probability of one thing being true given that another thing is true. Given a hypothesis $H$ and evidence $E$, Bayes' theorem states that the relationship between the probability of the hypothesis before getting the evidence $P(H)$ and the probability of the hypothesis after getting the evidence $P(H|E)$ is:

$$P(H|E) = \frac{P(E|H)}{P(E)} P(H) \tag{9.7}$$

where the quotient $P(E|H)/P(E)$ represents the support $E$ provides for $H$. Note that the Bayes' theorem holds also if the probabilities are represented by probability density functions, as postulated in the Bayesian approach. Here the probability is no longer an expected frequency and rather represents the degree of belief, or measure of plausibility, about the occurrence of the next event given incomplete knowledge. This may well be the case of an unrest episode at a volcano. Subjective probability is estimated in a different way from the frequentist probability. The best procedure is through the formalization of the degree of belief of a group of scientists (intersubjective probability), which tends to be much more coherent than that of a single researcher and also evaluates the epistemic uncertainty from multiple perspectives, increasing the likelihood of considering a fuller range of information. The most accepted procedure of eliciting a degree of belief is the Delphi method, which relies on a

structured panel of experts where information is fed back in summary form, allowing the panel to discuss and revise assessments several times, with opinions usually kept anonymous. Experts' opinions may be weighted according to the experience of the participants (Aspinall 2006; Marzocchi and Bebbington 2012).

Therefore, objective and subjective probabilities correspond to two different approaches to estimate uncertainty, which are expected to converge towards the same results when many data are available. The latter condition is often not met, hindering the use of the frequentist approach and hence requiring the use of Bayesian probability.

Probabilistic forecast considers the possibility of occurrence of an eruption both on the long- and short-term. The shift from long- to short-term forecast is determined by whether or not there are anomalous monitoring observations. Without anomalous monitoring data, probabilistic forecasts are made on the basis of the past eruption history of the volcano. Both time windows are discussed below.

### 9.7.1 Long-Term Forecasting

Long-term eruption forecast commonly relies on a frequentist approach that is concerned with the quality and quantity of the available data on the past eruptions at a volcano. More data on the past eruptions do not necessarily lead to a better forecast, as inhomogeneity in the catalogue complicates the approach, and different eruption catalogues can lead to different eruption forecasts. The used data are historical and geological. Historical records are usually short, lasting no longer than a few centuries and often incomplete, particularly in the earlier part of the record, for small-scale eruptions or for unrest episodes (which are unrecorded in geological data), in case they failed to erupt. Geological data can go back to tens of thousands of years, although the geologic record also incompletely preserves evidence of smaller eruptions and burial of older deposits is common.

A first-order requisite in determining the type of long-term forecast model to be adopted is dictated by any evidence that the history of the volcano has been characterized by activity at statistically different levels (or rates) in different intervals. If this condition is not met, a **stationary** model (whose parameters do not change with time) may be used. Otherwise, a **non-stationary** model, which involves trend(s) or level changes in parameters and hence in activity, may be preferred (Marzocchi and Bebbington 2012). Stationary models constitute a sort of maximum ignorance alternative, as lacking any information about the temporal evolution of the activity. Moreover, as incorporating an incorrect non-stationary model leads to greater bias, stationary models are also more robust. The **Poisson process** is an example of stationary model that assumes that the distribution of the remainder of the repose length is independent of the elapsed repose length. This is a memoryless property and implies that nothing is known about the temporal structure of the process, except the mean return period. The Poisson process is a good model for describing phenomena where the probability of occurrence is small and constant. In the Poisson process with $n$ events in $\tau$ unit time intervals, the parameter $\lambda = n/\tau$ is the expected average rate of events, i.e., the reciprocal of the average return period. For a Poisson distribution, the probability of observing $k$ events (for example eruptions) in a time interval $t$ is given by:

$$P(k,\lambda) = \frac{\lambda^k e^{-\lambda}}{k!} \tag{9.8}$$

The model also indicates that the probability of an event occurring at time $T$ within a time interval $\delta t$ is:

$$P(t < T < t + \delta t) = 1 - e^{-\lambda \delta t} \tag{9.9}$$

providing a useful approach to define the probability of an eruption in a given time.

A basic principle of the Poisson process is that events occur independently. However, in several cases a dependency between events can be postulated: for example, one can assume that the

previous eruption influences the timing of the next eruption onset. In this case, taking into account for the size of the previous event leads to a **time-predictable model**, which assumes a constant rate of magma input, so that eruption occurs when a critical level of magma is reached (Burt et al. 1994). Thus, the repose length depends on the volume of only the most recent eruption. An example of time-predictable behaviour is shown by the recent eruptive history of the Axial Seamount caldera (Juan de Fuca Ridge; Fig. 8.17; Nooner and Chadwick 2016). Here, given a critical threshold (the level of inflation) for eruptions, one can evaluate the time needed to reach again the threshold. With a size-dependent model the possible size of future events is conditioned on the prior eruptive history. In the case of a **size-predictable behaviour**, given a general volumetric threshold, one can consider the elapsed time from the last eruption and estimate the expected size of the next eruption as a function of time on a cumulative curve, as for example illustrated for the recent eruptive history of Akan volcano, Japan (Fig. 9.19; Hasegawa and Nakagawa 2016).

Long-term eruption forecast usually focuses on the eruptive record of a single volcano. However, in some cases, regional or global estimates are made, including the probability to have eruption as a function of its VEI for different exposure times (Pyle 1998; Martin et al. 2004; Mason et al. 2004; Sandri et al. 2004; Papale and Marzocchi 2019). The global probabilities are based on the frequency of the eruptions as a function of the VEI, which follows an overall power law behaviour, with many smaller-size events and fewer larger-size events (Fig. 1.14b). In this frame, the largest explosive eruptions have a longer repose time (or time elapsed from the previous eruption) than moderate eruptions. This implies that large explosive eruptions require a longer time to recharge the magmatic system and accumulate a sufficiently large amount of gas. Interestingly, the global probability to have a VEI 8 eruption, which can be considered the most destructive natural event of our planet, in our lifetime may be orders of magnitude larger than other events considered relatively remote in our everyday life (Fig. 9.20).

These global long-term statistical approaches also reveal different behaviours for volcanoes with open conduit compared to those with closed conduit. Open conduit systems seem to follow a time-predictable model, with a marked time clustering of events, whereas closed conduit systems seem to have no significant tendency

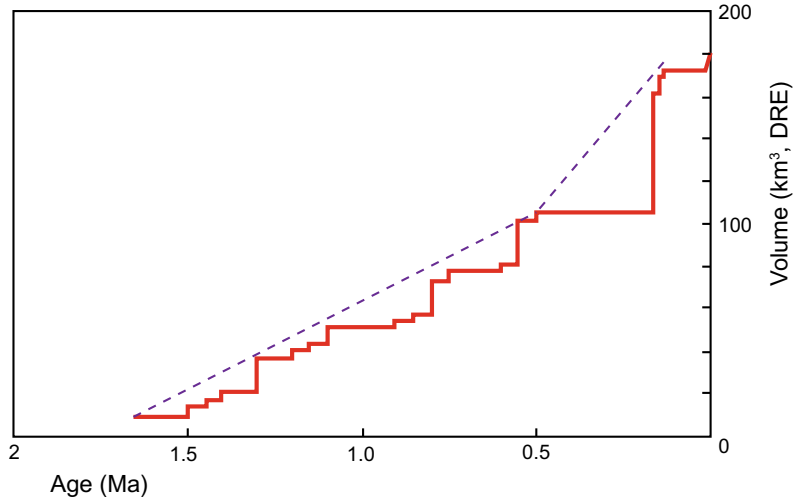


**Fig. 9.19** Age versus cumulative volume of eruptive groups and post-caldera explosive eruptions of Akan volcano (Japan). Dashed line is the volume-predictable line (modified after Hasegawa and Nakagawa 2016). In this case, the line shows a variation through time

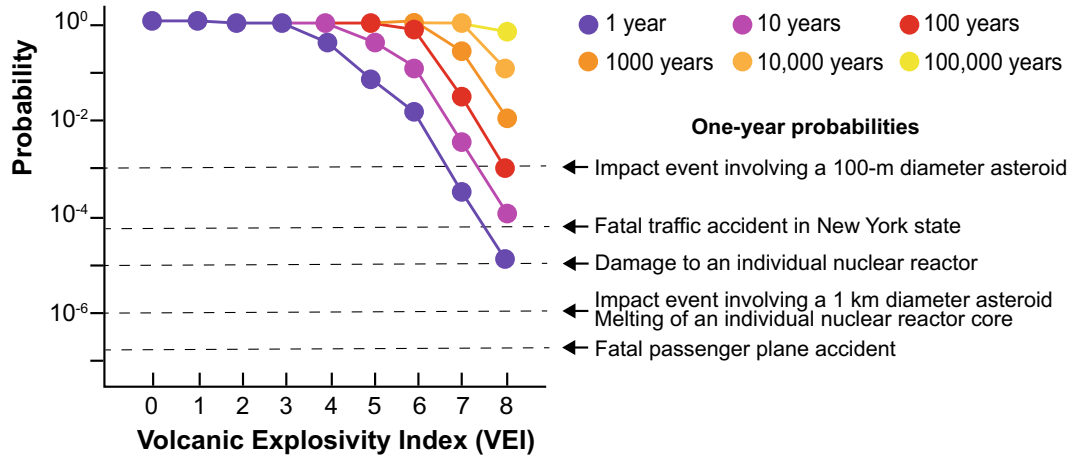


**Fig. 9.20** The probability of at least one eruption of a given VEI size on Earth is shown over different time intervals from 1 to 100,000 years. The 1-year probabilities of these events are compared to those for other threats (modified after Papale and Marzocchi 2019)

toward a size- or a time-predictable model, and the eruptions mostly follow a Poisson distribution (Marzocchi and Zaccarelli 2006). However, these global-scale results may be only partly consistent with evidence at regional scale. For example, while Indonesian open conduit volcanoes show no evidence of size-predictable behaviour, closed conduit volcanoes show a significant probability (>0.999) that the VEI of the next eruption increases with increasing repose length, supporting size-predictability (Bebbington 2014). Despite any regional variation, these results are useful in building general probabilistic models for volcanic hazard assessment of open and closed conduit systems. Magma composition is a further feature statistically affecting repose and unrest times. In particular, high silica, and thus high viscosity, felsic systems have longer repose and duration of precursory activity and tend to erupt larger quantities of material (Passarelli and Brodsky 2005).

A limitation of long-term eruption forecast is that this is commonly achieved only considering the reported (description-based) eruptive history of a volcano, rather than understanding the possible processes (physics-based) responsible for the eruptive record. This limitation, while not introducing any bias, may significantly affect forecast estimates, not only in time, but also in space, concerning the forecast of the location of the possible eruptive vent (Connor et al. 2003). This latter possibility holds especially true for volcanoes without central conduit, as calderas, where the location of a future vent is more uncertain. Nevertheless, new approaches are considering the mechanical conditions controlling the shallow transfer of magma below calderas, allowing moving from empirical pattern recognition to models based on the physics behind the patterns to define the location of future vents (see Sect. 5.9; Rivalta et al. 2019).

### 9.7.2 Short-Term Forecasting

For obvious reasons, most of the attention in forecasting eruptions has been given to the short-term forecast, which is based on the monitoring data collected during unrest. In fact, during unrest any long-term probability based on the past frequency of eruptions becomes less important than what is being observed from the monitoring signals.

In the case of frequently erupting volcanoes (that is, with open conduit) and available monitoring record, a frequentist approach may be used (Marzocchi and Bebbington 2012). For example, the probability $P(T)$ of occurrence of eruption

based on the appearance of a certain monitoring precursor (or hit rate) is:

$$P(T) = n_p/N \tag{9.10}$$

where $n_p$ is the number of eruptions anticipated by the precursor in an arbitrary time window $t$ and $N$ is the total number of eruptions. The probability $P(F)$ to have a false alarm using the same precursor (false alarm rate) is given by:

$$P(F) = (m - n_p)/m \tag{9.11}$$

where $m$ is the number of times in which the precursor has been observed. Retrospective testing for this approach has shown a large variability in the results, with $P(T)$ from 60 to 100%, and $P(F)$ from 20 to 60%.

However, most volcanoes, including the high-risk ones, have closed conduit, and, not having erupted in the last decades, have hindered the creation of the eruptive unrest database required by the frequentist approach. Vesuvio, which last erupted in 1944 and has been in a continuous state of quiescence ever since, is an example of volcano with this behaviour. As a result of the lack of eruptive unrest databases, short-term eruption forecast at closed conduit volcanoes has to make use of unavoidable expert opinion and relies on a Bayesian approach based on current monitoring data, or on data from analogue volcanoes (i.e., volcanoes with similar behaviour; e.g., Marzocchi et al. 2004b). In this context, the monitoring anomalies acquire a status of eruptive precursors. While precursors in science are often interpreted in a deterministic (certain) sense, in volcanology, because of the general lack of a one-to-one correlation between precursors and eruptions, the possible observation of precursors should be more realistically translated into an increased probability of eruption (Marzocchi and Bebbington 2012). As anticipated, in volcanoes with closed conduit the most reliable indicators of impending eruption remain the multi-parametric data indicating shallow dike propagation.

Converting the detection of possible precursors into the probability of eruption is challenging (e.g., Anderson and Poland 2016). The scarce amount of past data and the limited knowledge of the pre-eruptive physical processes hinder solving the hazard/risk problem with a rigorous and testable scientific model. Nevertheless, the structured solving approach required by the risk associated with eruption may be supported by treating scientific uncertainty in a fully systematized manner, using Bayesian statistics. This is achieved driving the opinion of experts in a formal and transparent probabilistic procedure with quantitative decision-making protocols, which are prepared before a crisis and consist of quantitative rules that can justify each step of the decision-making process (Marzocchi et al. 2004b; Marzocchi and Bebbington 2012). This procedure is based on the evidence that, when scientists asked to make a forecast limit their estimates to those that they think are really likely, the final results are usually within a single order of magnitude.

Examples of these structured approaches translating the observation of one or more possible precursors into a probabilistic assessment using expert opinion are elicitations, Bayesian belief networks and Bayesian event trees.

**Elicitations** are techniques to gather information from scientists who give their opinion on a specific topic. In volcanology this usually regards the state of a volcano during unrest, the probability to have eruption and the identification of thresholds, usually as orders of magnitude, in the monitoring parameters to define specific behaviours, to be also included in Bayesian event trees (Cooke et al. 1991; Aspinall 2006; Selva et al. 2012). Elicitations may be run in meetings or online, and are usually preceded by an informative meeting and followed by a discussion meeting.

Bayesian belief networks and event trees have a similar structure, representing a general quantitative framework where all relevant monitoring observations are embedded into a probabilistic

scheme through expert opinion, conceptual models and any monitoring data. In particular, a **Bayesian Belief Network** is a graphical representation of relevant observations (nodes) and their causal links (Fig. 9.21; Aspinall et al. 2003, 2006; Hincks et al. 2014). Associated with each node is a set of conditional probabilities that describe the relationship between the states of the variable at the node with the states of the other variables at connected nodes. These conditional probabilities are then combined through the Bayes' theorem to get the probability of any specific event. Bayesian Belief Networks are also used for retrospective analysis, as for the explosion at Galeras (Colombia) volcano in 1993 and for the 1975–1977 unrest at La Soufriere, in the latter case demonstrating that a formal evidential frame could have supported the authorities' concerns about public safety and decision to evacuate (Hincks et al. 2014).

A **Bayesian Event Trees** (BET) is a framework for discussing probabilities of possible outcomes of unrest, with each branch of the tree leading from a necessary prior event to a more specific outcome (e.g., Newhall and Hoblitt 2002). In particular, a BET is a graphical, tree-like representation of events in which branches are logical steps from a general prior event through increasingly specific subsequent events (intermediate outcomes) to final outcomes. These events, or nodes, include the inferred nature and outcome of unrest, and the inferred size and type of the possible eruption. Due to their Bayesian nature, at each node the probability density functions for the successive nodes are quantified, and aleatoric and epistemic uncertainties acknowledged and, if possible, quantified (Fig. 9.22). Therefore, a BET does not rule out any possibility, but it shapes the probability distribution of the event considered around the most likely outcome, accounting for all available data. Indeed, a BET is structured to merge any kind of information, including theoretical models of the eruptive process, past (historical and geological) and monitoring data (Marzocchi et al., 2004b,2008). Bayesian Event Trees have been used for several decades at many volcanoes, including Mount St. Helens, Pinatubo, Soufrière Hills (Montserrat), Popocatépetl (Mexico), Sinabung (Indonesia), Guagua Pichincha and Tungurahua (Ecuador; Newhall and Hoblitt 2002; Wright et al. 2019).

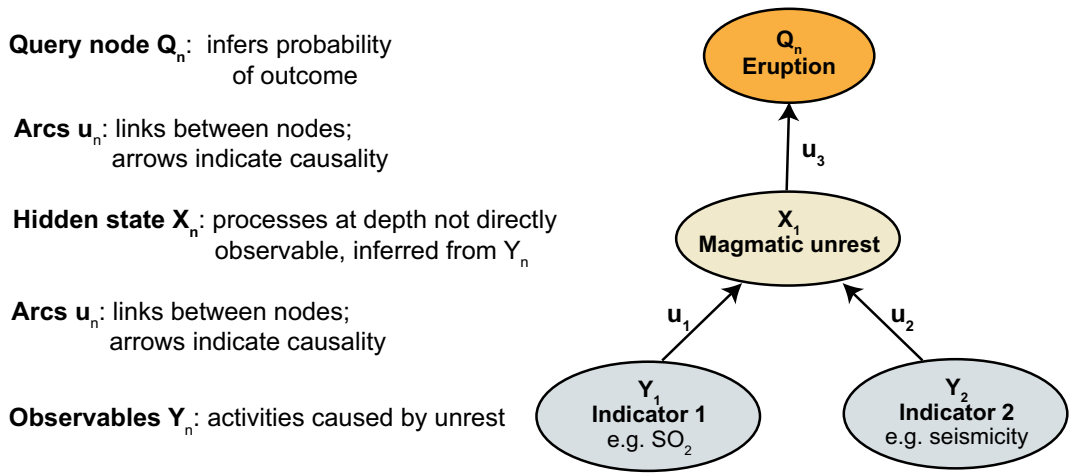


**Fig. 9.21** Elementary Bayesian Belief Network (BNN) representing a simple volcanological model to infer the probability of eruption resulting from unrest. Unrest must be inferred from observables Y (e.g., seismicity and $SO_2$ emission). The query node (eruption) is the outcome of interest. *Y* = set of observables, *X* = set of unobserved states, *u* = set of directed links between nodes. Arrows indicate direction of causality or influence. For the simple case where nodes are assigned discrete states, node relationships are described by conditional probability tables (modified after Hincks et al. 2014)

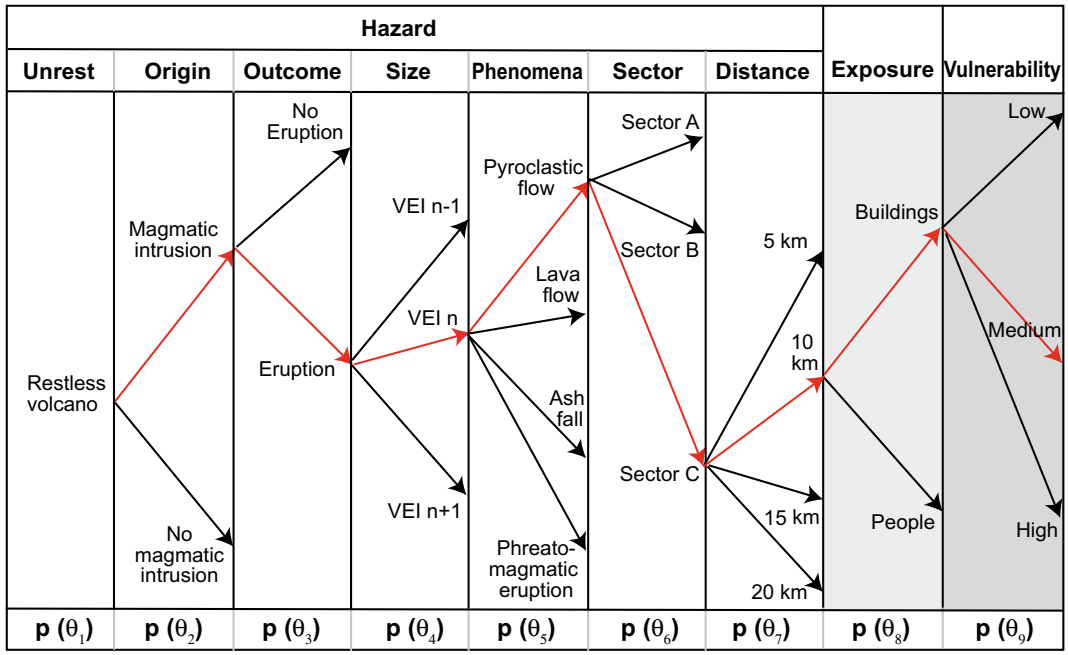


**Fig. 9.22** Sketch of a Bayesian Event Tree (BET). The nine steps progress from general to more specific events, involving the hazard, exposure and vulnerability components. The selected path (red arrows) is characterized by a probability $p(\theta_n)$ at each step (modified after Marzocchi et al. 2004b)

Additionally, BETs have been used for real-time eruption forecast of quiescent volcanic areas without historical activity, for which otherwise limited prior information is available, as the Auckland Volcanic Field (New Zealand; Lindsay et al. 2010). Event trees may be also used for long-term forecast, as for example at the Teide-Pico Vejo volcanoes of Tenerife (Canary Islands): here the BET was based on the geological, historical, geophysical and volcanological knowledge, with the possibility of including short-term monitoring data (Martì et al. 2008). Finally, BETs have been applied in real-time during simulation exercises (as in New Zealand and Dominica; Lindsay et al. 2010; Sandri et al. 2017b) or have been even applied retrospectively, as for the 1631 Vesuvio eruption and the 1982–1984 unrest at Campi Flegrei (Sandri et al. 2009; Selva et al. 2012). Application to Vesuvio suggests that the pre-eruptive signals that significantly increased the probability of the 1631 eruption could have been likely detected more than 2 months in advance, providing satisfactory forecast. At Campi Flegrei the probabilities associated with the first three nodes of the BET have been estimated for the 1982–1984 unrest, when the appearance of surface fractures in 1983 increased the eruptive probability to ~40% as best-guess value, although affected by a large uncertainty (the 80% confidence interval was 0.3–91%).

## 9.8 Summary

Unrest is defined by evident geodetic, geophysical and geochemical variations in the monitoring signals, which may anticipate a possible eruption. Unrest commonly results from shallow magma accumulation or transfer, although a remote seismic trigger, responsible for dynamic and static stress variations, or the pressurization of a hydrothermal system may also promote unrest. Defining the processes occurring during unrest is fundamental to understand volcanoes and may also allow effective eruption forecast.

However, the limited knowledge of unrest processes and the lack of real precursors confine any forecast to the identification of the states of an active volcano and the statistical analysis of the monitoring parameters. In the first case, the monitoring parameters may indicate a state of magma accumulation or magma transfer. Magma transfer is related to shallow dike propagation and accompanied by distinctive monitoring signals, as deformation with non-radial symmetry and possible upward propagating seismicity. Because shallow dike propagation may feed eruption, its real-time detection should be the ultimate target of any monitoring system. In the second case, the statistical analysis of unrest monitoring data feeds short-term eruption forecast models. These have progressed from a deterministic to a dominantly probabilistic approach as a result of the overall lack of reliable and ubiquitous precursors. Multi-parametric monitoring data are currently incorporated, especially at closed conduit volcanoes, in several Bayesian forecasting tools, as elicitations, Bayesian Belief Networks and Bayesian Event Trees. Short-term forecast may also exploit a frequentist probabilistic approach at open conduit volcanoes, if monitoring data on previous eruptive unrest are available. The frequentist approach is otherwise widely used for long-term forecast, relying on historical or geologic data. In addition to forecasting eruptions, volcanologists take other actions to assess volcanic hazard to mitigate risk. These include the definition of hazardous scenarios (including the reference eruption), the establishment of early warning systems and the issuance of volcano alert levels.

## 9.9 Main Symbols Used

| | |
|---|---|
| $A$ | event |
| $s$ | distance |
| $E$ | evidence |
| $H$ | hypothesis |
| $j$ | amplitude term |
| $K$ | constant |
| $k$ | number of events |
| $M$ | magnitude |
| $m$ | number of times in which the precursor has been observed |
| $N$ | number of opportunities or eruptions |
| $n$ | number of times an event occurs |
| $n_p$ | number of eruptions anticipated by the precursor |
| $p$ | power law exponent |
| $P$ | probability |
| $P(F)$ | probability of false alarm rate |
| $P(T)$ | probability of hit rate |
| $P_{EQ}$ | extra pressure generated by the earthquake |
| $t$ | time |
| $t_f$ | time of failure |
| $T$ | time of occurrence |
| $T_{EQ}$ | time between large earthquakes |
| $T_v$ | ordinary recurrence time of volcanic eruptions |
| $X_t$ | fraction of eruptions triggered by earthquakes |
| $\alpha$ | constant |
| $\Delta C_{FS}$ | Coulomb failure stress |
| $\Delta P$ | pore pressure change |
| $\Delta P_{\mathrm{m}}$ | overpressure required to nucleate a dike |
| $\Delta\sigma_N$ | normal stress change |
| $\Delta\sigma_S$ | shear stress change |
| $\lambda$ | average rate of events |
| $\mu$ | coefficient of friction |
| $\tau$ | unit time intervals |
| $\Omega$ | monitoring variable |

## References

Acocella V, Behncke B, Neri M, D'Amico S (2003) Link between major flank slip and 2002–2003 eruption at Mt. Etna (Italy). Geophys Res Lett 30:2286. https://doi.org/10.1029/2003GL018642

Acocella V (2014) Great challenges in volcanology: how does the volcano factory work? Front Volcanol 2:1–10. https://doi.org/10.3389/feart.2014.00004

Acocella V, Di Lorenzo R, Newhall C, Scandone R (2015) An overview of recent (1988 to 2014) caldera unrest: knowledge and perspectives. Rev Geophys 53: https://doi.org/https://doi.org/10.1002/2015RG000492

Albino F, Biggs J, Syahbana DK (2019) Dyke intrusion between neighbouring arc volcanoes responsible for 2017 pre-eruptive seismic swarm at Agung. Nat Commun 10:748. https://doi.org/10.1038/s41467-019-08564-9

Albright JA, Gregg PM, Lu Z, Freymueller JT (2019) Hindcasting magma reservoir stability preceding the 2008 eruption of Okmok, Alaska. Geophys Res Lett 46:8801–8808

Almendros J, Carmona E, Jimenez V, Diaz-Moreno A, Lorenzo F (2018) Volcano-tectonic activity at Deception Island volcano following a seismic swarm in the Bransfield Rift (2014–2015). Geophys Res Lett 45:4788–4798

Anderson KR, Poland MP (2016) Bayesian estimation of magma supply, storage, and eruption rates using a multiphysical volcano model: Kılauea Volcano, 2000–2012. Earth Planet Sci Lett 447:161–171

Arzilli F, Morgavi D, Petrelli M, Polacci M, Burton M, Di Genova D (2019) The unexpected explosive sub-Plinian eruption of Calbuco volcano (22–23 April 2015; southern Chile): triggering mechanism implications. J Volcanol Geoth Res 378:35–50

Aspinall WP, Woo G, Voight B, Baxter PJ (2003) Evidence-based volcanology: application to eruption crises. J Volcanol Geoth Res 128:273–285

Aspinall W (2006) Structured elicitation of expert judgment for probabilistic hazard and risk assessment in volcanic eruptions. In: Mader H, Coles S, Connor C, Connor L (eds) Statistics in volcanology. Geological Society of London on behalf of IAVCEI London, pp 15–30

Aspinall WP, Carniel R, Jaquet O, Woo G, Hincks T (2006) Using hidden multi-state Markov models with multi-parameter volcanic data to provide empirical evidence for alert level decision-support. J Volcanol Geoth Res 153:112–124

Barberi F, Martini M, Rosi M (1990) Nevado del Ruiz volcano (Colombia): pre-eruption observations and the November 13, 1985 catastrophic event. J Volcanol Geoth Res 42:1–12

Battaglia M, Roberts CW, Segall P (1999) Magma intrusion beneath Long Valley caldera confirmed by temporal changes in gravity. Science 285:2119–2122

Bebbington M (2009) Volcanic eruptions: stochastic models of occurrence patterns. In: Meyers B (ed) Encyclopedia of complexity and system science, vol 9. Springer New York, pp 9831–9861

Bebbington MS (2014) Long-term forecasting of volcanic explosivity. Geophys J Int 197:1500–1515

Bebbington MS, Jenkins FS (2019) Intra-eruption forecasting. Bull Volcanol 81:34

Belardinelli ME, Bozzarri A, Cocco M (2003) Earthquake triggering by static and dynamic stress changes. J Geophys Res 108:2135. https://doi.org/10.1029/2002JB001779

Bell AF, Greenhough J, Heap MJ, Main IG (2011) Challenges for forecasting based on accelerating rates of earthquakes at volcanoes and laboratory analogues. Geophys J Int 185:718–723

Benito-Saz MA, Sigmundsson F, Charco M, Hooper A, Parks M (2019) Magma flow rates and temporal evolution of the 2012–2014 post eruptive intrusions at El Hierro, Canary Islands. J Geophys Res 124 https://doi.org/https://doi.org/10.1029/2019JB018219

Biggs J, Robertson E, Cashman K (2016) The lateral extent of volcanic interactions during unrest and eruption. Nat Geosci 9:308–311

Burt ML, Wadge G, Scott WA (1994) Simple stochastic modelling of eruption history of basaltic volcano: Nyamuragira, Zaire. Bull Volcanol 56:87–97

Cassidy M, Ebmeier SK, Helo C, Watt SFL, Caudron C, Odell A et al (2019) Explosive eruptions with little warning: experimental petrology and volcano monitoring observations from the 2014 eruption of Kelud, Indonesia. Geochem Geophys Geosyst 20:4218–4247

Caudron C, Girona T, Taisne B, Suparjan, Gunawan H, Kristianto et al (2019) Change in seismic attenuation as a long-term precursor of gas-driven eruptions. Geology 47:632–636

Chesley C, LaFemina PC, Puskas C, Kobayashi D (2012) The 1707 Mw8.7 Hoei earthquake triggered the largest historical eruption of Mt. Fuji. Geophys Res Lett 39:L24309. https://doi.org/https://doi.org/10.1029/2012GL053868

Chiodini G, Vandemeulebrouck J, Caliro S, D'Auria L, De Martino P, Mangiacapra A et al (2015) Evidence of thermal-driven processes triggering the 2005–2014 unrest at Campi Flegrei caldera. Earth Planet Sci Lett 414:58–67

Chiodini G, Paonita A, Aiuppa A, Costa A, Caliro S, De Martino P et al (2016) Hotter volcanic unrest for magmas near the critical degassing pressure. Nat Commun 7:13712. https://doi.org/10.1038/ncomms13712

Connor CB, Sparks RSJ, Mason RM, Bonadonna C, Young SR (2003) Exploring links between physical and probabilistic models of volcanic eruptions: the Soufriere Hills Volcano. Montserrat. Geophys Res Lett 30:1701. https://doi.org/10.1029/2003GL017384

Cooke RM (1991) Experts in uncertainty: opinion and subjective probability in science. Oxford Univ Press, New York, p 336

Crider JG, Frank D, Malone SD, Poland MP, Werner C, Caplan J (2011) Magma at depth: a retrospective analysis of the 1975 unrest at Mount Baker, Washington, USA. Bull Volcanol 73:175–189

D'Auria L, Pepe S, Castaldo R, Giudicepietro F, Macedonio G, Ricciolino P et al (2015) Magma injection beneath the urban area of Naples: a new mechanism for the 2012–2013 volcanic unrest at Campi Flegrei caldera. Sci Rep 5:13100. https://doi.org/10.1038/srep13100

D'Auria L, Barrancos J, Padilla GD, Pérez NM, Hernández PA, Melián G et al (2019) The 2016 Tenerife (Canary Islands) long-period seismic swarm. J Geophys Res 124:8739–8752

de Vita S, Sansivero F, Orsi G, Marotta E, Piochi M (2010) Volcanological and structural evolution of the Ischia resurgent caldera (Italy) over the past 10 ka. In: Groppelli G, Viereck L (eds) Stratigraphy and geology in volcanic areas. GSA Book Series Special Paper, vol 464, pp 193–239

Druitt TH, Costa F, Deloule E, Dungan M, Scaillet (2012) Decadal to monthly timescales of magma transfer and

reservoir growth at a caldera volcano. Nature 482:77–80
Eggert S, Walter TR (2009) Volcanic activity before and after large tectonic earthquakes: observations and statistical significance. Tectonophysics 471:14–26
Farquharson JI, Amelung F (2020) Extreme rainfall triggered the 2018 rift eruption at Kīlauea Volcano. Nature 580:491–495
Gaddes M, Hooper A, Bagnardi M, Inman H, Albino F (2018) Blind signal separation methods for InSAR: the potential to automatically detect and monitor signals of volcanic deformation. J Geophys Res 123:10226–10251
Galetto F, Acocella V, Caricchi L (2017) Caldera resurgence driven by magma viscosity contrasts. Nat Commun 8:1750. https://doi.org/10.1038/s41467-017-01632-y
Galetto F, Bagnardi M, Acocella V, Hooper A (2019) Noneruptive unrest at the caldera of Alcedo Volcano (Galápagos Islands) revealed by InSAR data and geodetic modelling. J Geophys Res 124. https://doi.org/https://doi.org/10.1029/2018JB017103
Gardine M, West M, Werner C, Doukas M (2011) Evidence of magma intrusion at Fourpeaked volcano, Alaska in 2006–2007 from a rapid-response seismic network and volcanic gases. J Volcanol Geoth Res 200:192–200
Giudicepietro F, Macedonio G, Martini M (2017) A physical model of sill expansion to explain the dynamics of unrest at Calderas with application to Campi Flegrei. Front Earth Sci 5:54. https://doi.org/10.3389/feart.2017.00054
Gregg CE, Houghton B, Ewert JW (2015) Volcano warning systems. In: Sigurdsson H, Houghton B, Rymer H, Stix J (eds) The encyclopaedia of volcanoes, 2nd edn. Academic Press, pp 1173–1186
Hamling IJ, Kilgour G (2020) Goldilocks conditions required for earthquakes to trigger basaltic eruptions: evidence from the 2015 Ambrym eruption. Sci Adv 6: eaaz5261
Harris RA (1998) Introduction to a special section: stress triggers, stress shadows, and implications for seismic hazards. J Geophys Res 103:24347–24358
Hasegawa T, Nakagawa M (2016) Large scale explosive eruptions of Akan volcano, eastern Hokkaido, Japan: a geological and petrological case study for establishing tephro-stratigraphy and -chronology around a caldera cluster. Quatern Int 397:39–51
Hincks TK, Komorowski J-C, Sparks RSJ, Aspinall WP (2014) Retrospective analysis of uncertain eruption precursors at La Soufrière volcano, Guadeloupe, 1975–77: volcanic hazard assessment using a Bayesian belief network approach. J Appl Volcanol 3:3
Hill DP, Pollitz F, Newhall C (2002) Earthquake-volcano interactions. Phys Today 55:41–47
Hill DP, Prejean SG (2007) Dynamic triggering Treatise of Geophysics, vol 4. Elsevier Amsterdam, pp 293–320
Jaquet O, Carniel R, Sparks S, Thompson G, Namar R, Di Cecca M (2006) DEVIN: A forecasting approach using stochastic methods applied to the Soufriere Hills Volcano. J Volcanol Geoth Res 153:97–111
Jellinek AM, DePaolo DJ (2003) A model for the origin of large silicic magma chambers: precursors of caldera-forming eruptions. Bull Volcanol 65:363–381
Kato A, Terkawa T, Yamanaka Y, Maeda Y, Horikawa S, Matsuhiro K (2015) Preparatory and precursory processes leading up to the 2014 phreatic eruption of Mount Ontake. Japan. Earth Plan Space 67:111
Kilburn CRJ (2003) Multiscale fracturing as a key to forecasting volcanic eruptions. J Volcanol Geoth Res 125:271–289
Kilburn CRJ, Sammonds PR (2005) Maximum warning times for imminent volcanic eruptions. Geophys Res Lett 32:L24313. https://doi.org/10.1029/2005GL024184
Kilburn RJ, de Natale G, Carlino S (2017) Progressive approach to eruption at Campi Flegrei caldera in southern Italy. Nat Commun 8:15312. https://doi.org/10.1038/ncomms15312
Kilburn CRJ (2018) Forecasting volcanic eruptions: beyond the failure forecast method. Front Earth Sci 6:133. https://doi.org/10.3389/feart.2018.00133
King C-Y, Basler D, Presser TS, Evans CW, White LD, Minissale AD (1994) In search of earthquake-related hydrologic and chemical changes along the Hayward fault. Appl Geochem 9:83–91
Koulakov I, Smirnov SZ, Gladkov V, Kasaktina E, West M, El Khrepy S et al (2018) Causes of volcanic unrest at Mt. Spurr in 2004–2005 inferred from repeated tomography. Sci Rep 8:17482. https://doi.org/https://doi.org/10.1038/s41598-018-35453-w
Linde AT, Sacks IS, Johnston MJS, Hill DP, Bilham RG (1994) Increased pressure from rising bubbles as a mechanism for remotely triggered seismicity. Nature 371:408–410
Linde AT, Sacks IS (1998) Triggering of volcanic eruptions. Nature 395:888–890
Lindsay J, Marzocchi W, Jolly G, Constantinescu R, Selva J, Sandri L (2010) Towards real-time eruption forecasting in the Auckland Volcanic Field: application of BET_EF during the New Zealand National Disaster Exercise 'Ruaumoko.' Bull Volcanol 72:185–204
Lipman PW, Mullineaux DR (eds) (1981) The 1980 eruptions of Mount St. Helens, Washington. US Geological Survey Professional Paper 1250, 844 p
Lopez C, Blanco MJ, Abella R, Brenes B, Cabrera Rodriguez VM, Casas B (2012) Monitoring the volcanic unrest of El Hierro (Canary Islands) before the onset of the 2011–2012 submarine eruption. Geophys Res Lett 39:L13303. https://doi.org/10.1029/2012GL051846
Manga M, Brodsky E (2006) Seismic triggering of eruptions in the far field: volcanoes and geysers. Ann Rev Earth Planet Sci 34:263–291
Manga M (2020) When it rains, lava pours. Nature 580:457–458
Martì J, Aspinall WP, Sobradelo R, Felpeto A, Geyer A, Ortiz R et al (2008) A long-term volcanic hazard event

tree for Teide-Pico Viejo stratovolcanoes (Tenerife, Canary Islands). J Volcanol Geoth Res 178:543–552
Martin AJ, Umeda K, Connor CB, Weller JN, Zhao D, Takahashi M (2004) Modeling long-term volcanic hazards through Bayesian inference: an example from the Tohoku volcanic arc. Japan. J Geophys Res 109: B10208. https://doi.org/10.1029/2004JB003201
Marzocchi W (2002) Remote seismic influence on large explosive eruptions. J Geophys Res 107:2018
Marzocchi W, Zaccarelli L, Boschi E (2004a) Phenomenological evidence in favour of a remote seismic coupling for large volcanic eruptions. Geophys Res Lett 31:L04601
Marzocchi W, Sandri L, Gasparini P, Newhall C, Boschi E (2004b) Quantifying probabilities of volcanic events: the example of volcanic hazard at Mt. Vesuvius. J Geophys Res 109:B11201. https://doi.org/10.1029/2004JB003155
Marzocchi W, Zaccarelli L (2006) A quantitative model for the time-size distribution of eruptions. J Geophys Res 111:B04204. https://doi.org/10.1029/2005JB003709
Marzocchi W, Woo G (2007) Probabilistic eruption forecasting and the call for an evacuation. Geophys Res Lett 34:L22310
Marzocchi W, Sandri L, Selva J (2008) BET_EF: a probabilistic tool for long- and short-term eruption forecasting. Bull Volcanol 70:623–632
Marzocchi W, Bebbington MS (2012) Probabilistic eruption forecasting at short and long time scales. Bull Volcanol 74:1777–1805
Marzocchi W, Garcia-Aristizabal A, Gasparini P, Mastellone ML, di Ruocco A (2012) Basic principles of multi-risk assessment: a case study in Italy. Nat Hazards 62:551–573
Mason BG, Pyle DM, Oppenheimer C (2004) The size and frequency of the largest explosive eruptions on Earth. Bull Volcanol 66:735–748
McNutt SR (2000) Volcanic seismicity. In: Sigurdsson H, Houghton B, McNutt S, Rymer H, Stix J (eds) The encyclopedia of volcanoes, 1st edn. Elsevier Academic Press, pp 1015–1034
McLeod P, Tait S (1999) The growth of dykes from magma chambers. J Volcanol Geoth Res 92:231–245
Montgomery DR, Manga M (2003) Streamflow and water well responses to earthquakes. Science 300:2047. https://doi.org/10.1126/science.1082980
Moran SC, Newhall C, Roman DC (2011) Failed magmatic eruptions: late-stage cessation of magma Ascent. Bull Volcanol 73:115–122
Namiki A, Rivalta E, Woith H, Willey T, Parolai S, Walter TR (2019) Volcanic activities triggered or inhibited by resonance of volcanic edifices to large earthquakes. Geology 47:67–70
Newhall CG, Dzurisin DD (1988) Historical unrest at large calderas of the world. US Geological Survey Professional Paper, 1109 p
Newhall CG, Punongbayan RS (1996) Fire and mud: eruptions and lahars of Mount Pinatubo, Philippines. Philippine Institute of Volcanology and Seismology, Quezon City and University of Washington Press Seattle and London, 1126 p
Newhall CG (2000) Volcano warnings In: Sigurdsson H, Houghton B, McNutt S, Rymer H, Stix J (eds) The encyclopaedia of volcanoes, 1st edn. Elsevier Academic Press, pp 1185–1198
Newhall CG, Hoblitt RP (2002) Constructing event trees for volcanic crises. Bull Volcanol 64:3–20
Newhall CG, Costa F, Ratdomopurbo A, Venezky DY, Widiwijayanti C, Thin Zar Win N (2017) WOVOdat—an online, growing library of worldwide volcanic unrest. J Volcanol Geoth Res 345:184–199
Nishimura T, Ueki S (2011) Seismicity and magma supply rate of the 1998 failed eruption at Iwate volcano, Japan. Bull Volcanol 73:133–142
Nishimura T (2017) Triggering of volcanic eruptions by large earthquakes. Geophys Res Lett 44:7750–7756
Nooner SL, Chadwick WW (2016) Inflation-predictable behavior and co-eruption deformation at Axial Seamount. Science 354:1399–1403
Nostro C, Stein RS, Cocco M, Belardinelli ME, Marzocchi W (1998) Two-way coupling between Vesuvius eruptions and southern Apennine earthquakes, Italy, by elastic stress transfer. J Geophys Res 103:24487–24504
Oikawa T, Yoshimoto M, Nakada S, Maeno F, Komori J, Shimano T et al (2016) Reconstruction of the 2014 eruption sequence of Ontake Volcano from recorded images and interviews. Earth Planets Space 68:79
Palmer J (2020) The volcanology revolution. Nature 581:256–259
Papale P (2017) Rational volcanic hazard forecasts and the use of volcanic alert levels. J Appl Volcanol 6:13
Papale P, Marzocchi W (2019) Volcanic threats to global society. Science 363:1275–1276
Parks MM, Biggs J, England P, Mather TA, Nomikou P, Palamartchouk K (2012) Evolution of Santorini Volcano dominated by episodic and rapid fluxes of melt from depth. Nat Geosci 5:749–754
Passarelli L, Brodsky EE (2005) The correlation between run-up and repose times of volcanic eruptions. Geophys J Int 188:1025–1045
Phillipson G, Sobradelo R, Gottsmann J (2013) Global volcanic unrest in the 21st century: an analysis of the first decade. J Volcanol Geoth Res 264:183–196
Poland MP, Anderson KR (2020) Partly cloudy with a chance of lava flows: forecasting volcanic eruptions in the twenty-first century. J Geophys Res 125: e2018JB016974. https://doi.org/https://doi.org/10.1029/2018JB016974
Potter SH, Scott BJ, Jolly GE, Neall VE, Johnston DM (2015) Introducing the Volcanic Unrest Index (VUI): a tool to quantify and communicate the intensity of volcanic unrest. Bull Volcanol 77:77
Pritchard ME, Jay JA, Aron F, Henderson ST, Lara LE (2013) Subsidence at southern Andes volcanoes induced by the 2010 Maule, Chile earthquake. Nat Geosci 6:632–636
Pyle DM (1998) Forecasting sizes and repose times of future extreme volcanic events. Geology 26:367–370

Ripepe M, Marchetti E, Delle Donne D, Genco R, Innocenti L, Lacanna G et al (2018) Infrasonic early warning system for explosive eruptions. J Geophys Res 123:9570–9585

Rivalta E, Corbi F, Passarelli L, Acocella V, Davis T, Di Vito MA (2019) Stress inversions to forecast magma pathways and eruptive vent location. Sci Adv 5: eaau9784

Robertson RM, Kilburn CRJ (2016) Deformation regime and longterm precursors to eruption at large calderas: Rabaul, Papua New Guinea. Earth Planet Sci Lett 438:86–94

Roman DC, Power JA (2011) Mechanism of the 1996–97 non-eruptive volcano-tectonic earthquake swarm at Iliamna Volcano, Alaska. Bull Volcanol 73:143–153

Sandri L, Marzocchi W, Zaccarelli L (2004) A new perspective in identifying the precursory patterns of eruptions. Bull Volcanol 66:263–275

Sandri L, Guidoboni E, Marzocchi W, Selva J (2009) Bayesian event tree for eruption forecasting (BET_EF) at Vesuvius, Italy: a retrospective forward application to the 1631 eruption. Bull Volcanol 71:729–745

Sandri L, Costa A, Selva J, Tonini R, Macedonio G, Folch A et al (2016) Beyond eruptive scenarios: assessing tephra fallout hazard from Neapolitan volcanoes. Sci Rep 6:24271. https://doi.org/10.1038/srep24271

Sandri L, Acocella V, Newhall C (2017a) Searching for patterns in caldera unrest. Geochem Geophys Geosyst 18. https://doi.org/https://doi.org/10.1002/2017GC006870

Sandri L, Tonini R, Rouwet D, Constantinescu R, Mendoza-Rosas AT, Andrade D et al (2017b) The need to quantify hazard related to non-magmatic unrest: from BET_EF to BET_UNREST. In: Gottsmann J, Neuberg, J, Scheu B (eds) Volcanic unrest: from science to society. IAVCEI Advances in Volcanology Springer, pp 63–82

Selva J, Orsi G, Di Vito MA, Marzocchi W, Sandri L (2012) Probability hazard map for future vent opening at the Campi Flegrei caldera, Italy. Bull Volcanol 74:497–510

Selva J, Acocella V, Bisson M, Costa A, Caliro S, De Martino P et al (2019) Volcanic and related hazards at Ischia (Italy): state of knowledge and future perspectives. J Appl Volcanol 8:5. https://doi.org/10.1186/s13617-019-0086-4

Sparks RSJ (2003) Frontiers: forecasting volcanic eruptions. Earth Planet Sci Lett 210:1–15

Sparks RSJ, Aspinall WP (2004) Volcanic activity: frontiers and challenges in forecasting, prediction and risk assessment. State Planet Front Challenges Geophys. Geophys Monogr 150. https://doi.org/https://doi.org/10.1029/150GM28

Stein RS (2003) Earthquake conversations. Sci Am 288:72–79

Stein RS (2004) Tidal triggering caught in the Act. Science 305:1248–1249

Syahbana DK, Kasbani K, Suantika G, Prambada O, Andreas AS, Saing UB (2019) The 2017–19 activity at Mount Agung in Bali (Indonesia): intense unrest, monitoring, crisis response, evacuation, and eruption. Sci Rep 9:8848. https://doi.org/10.1038/s41598-019-45295-9

Swanson DA, Casadevall TJ, Dzurisin D, Malone SD, Newhall CG, Weaver CS (1983) Predicting Eruptions at Mount St. Helens, June 1980 through December 1982. Science 221:1369–1376

Tait S, Jaupart C, Vergniolle S (1989) Pressure, gas content and eruption periodicity of a shallow crystallizing magma chamber. Earth Planet Sci Lett 92:107–123

Takada Y, Fukushima Y (2013) Volcanic subsidence triggered by the 2011 Tohoku earthquake in Japan. Nat Geosci 6:637–641

Tilling RI (1988) Lessons from materials science. Nature 332:108–109

Tilling RI (1989) Volcanic hazards and their mitigation: Progress and problems. Rev Geophys 27:237–269

Tizzani P, Battaglia M, Zeni G, Atzori S, Berardino P, Lanari R (2009) Uplift and magma intrusion at Long Valley caldera from InSAR and gravity measurements. Geology 37:63–66

Trasatti E, Acocella V, Di Vito MA, Del Gaudio C, Weber G, Aquino I et al (2019) Magma degassing as a source of long-term seismicity at volcanoes: the Ischia island (Italy) case. Geophys Res Lett 46. https://doi.org/https://doi.org/10.1029/2019GL085371

Voight B (1988) A method for prediction of volcanic eruptions. Nature 332:125–130

Voight B (1990) The 1985 Nevado del Ruiz volcano catastrophe: anatomy and retrospection. J Volcanol Geoth Res 44:349–386

Voight B, Cornelius RR (1991) Prospects for eruption prediction in near real-time. Nature 350:695–698

Walter TR, Troll VR, Cailleau B, Belousov A, Schmincke HU, Amelung F et al (2005) Rift zone reorganization through flank instability in ocean island volcanoes: an example from Tenerife, Canary Islands. Bull Volcanol 67:281–291

Walter TR, Amelung F (2007) Volcanic eruptions following M $\geq$ 9 megathrust earthquakes: implications for the Sumatra-Andaman volcanoes. Geology 35:539–542

Walter TR, Wang R, Acocella V, Neri M, Grosser H, Zschau J (2009) Simultaneous magma and gas eruptions at three volcanoes in southern Italy: an earthquake trigger? Geology 37:251–254

Wang CY, Manga M (2010) Hydrologic responses to earthquakes and a general metric. Geofluids 10:206–216

Werner CA, Doukas MP, Kelly PJ (2011) Gas emissions from failed and actual eruptions from Cook Inlet Volcanoes, Alaska, 1989–2006. Bull Volcanol 73:155–173

Wilson CJN (2008) Supereruptions and supervolcanoes: processes and products. Elements 4:29–34

Winson AEG, Costa F, Newhall CG, Woo G (2014) An analysis of the issuance of volcanic alert levels during volcanic crises. J Appl Volcanol 3:14

Witze A (2019) AI could help to predict eruptions. Nature 567:156–157
Wright HMN, Pallister JS, McCausland WA, Griswold JP, Andreastuti S, Budianto A (2019) Construction of probabilistic event trees for eruption forecasting at Sinabung volcano, Indonesia 2013–14. J Volcanol Geoth Res 382:233–252